SMHI

Meteorologi

Nr 126, 2007

Modelling of surface global radiation and CIE-weighted UV-radiation for the period 1980-2000

Anna Jansson and Weine Josefsson

Meteorologi
Nr 126, 2007

Modelling of surface global radiation and CIE-weighted UV-radiation for the period 1980-2000

P.1491.05

Anna Jansson and Weine Josefsson

Report Summary / Rapportsammanfattning

Issuing Agency/Utgivare	Report number/Publikation
Swedish Meteorological and Hydrological Institute S-601 76 NORRKÖPING Sweden	**126**
	Report date/Utgivningsdatum **March 2007**

Author (s)/Författare

Anna Jansson, Weine Josefsson

Title (and Subtitle/Titel

Modelling of surface global radiation and CIE-weighted UV-radiation for the period 1980-2000

Abstract/Sammandrag

This report presents the procedure for creation of surface global radiation and CIE-weighted UV-radiation for the years 1980-2000. The work was ordered by the Swedish Radiation Protection Authority (SSI) on behalf of "Miljömålsrådet". The created data covers a large geographical area over northwest Europe with a fine spatial (22x22 km) and temporal resolution (1 hour).

The input data are selected from the new version of the Rossby Centre regional atmospheric climate model (RCA3), ERA-40 (www.ecmwf.int/research/era) and observations.

For the creation of CIE-weighted UV-radiation, a clear sky model was first used and then a cloud modification model that reduces the clear sky radiation dependent on the cloud amount from the RCA3 model.

The report also includes a validation of the modelled CIE-weighted UV-radiation against independent observations. The root mean square deviation is for daily values about 38%, for monthly values, 13% and for yearly values 7%. Also a small bias toward higher modelled UV compared to observations exists in the data set.

For the creation of global radiation, the data has been selected from the RCA3 model with a correction made depended on the sun height. Also for the global radiation the validation results are presented in the report. The root mean square deviation is in the same order as for the modelled CIE-weighted UV-radiation, also here a small bias toward higher modelled values exist, but smaller then for the modelled CIE-weighted UV-radiation.

All CIE-weighted UV-radiation and global radiation created in this project are freely available for non-commercial usage at the web-interface, www.smhi.se/strang/omna. Here charts, fields and time series can be selected for hourly, daily, monthly and yearly values.

Key words/sök-, nyckelord

CIE-weighted UV-radiation, global radiation, cloud modification model

Supplementary notes/Tillägg	Number of pages/Antal sidor	Language/Språk
The work was ordered by the Swedish Radiation Protection Authority (SSI) on behalf of "Miljömålsrådet". (P.1491.05)	39	English

ISSN and title/ISSN och title

0347-2116 SMHI Reports Meteorology

Report available from/Rapporten kan köpas från:

SMHI
S-601 76 NORRKÖPING
Sweden

Contents

1 Introduction 1

2 Background 2

3 Data sources 3

3.1 ERA-40 3
3.2 The Rossby Centre regional atmospheric climate model 4
3.3 Observations 5
3.3.1 Ozone 5
3.3.2 UV-radiation 5
3.3.3 Global radiation 5

4 Calculation of CIE-weighted UV-radiation 6

4.1 Clear sky model 7
4.1.1 Input data 7
4.1.2 Results 11
4.2 Development of a cloud modification model 13
4.3 Results 19

5 Global radiation 23

5.1 Clear sky 23
5.2 All sky conditions 25

6 Available output data 28

7 Discussion and Conclusions 30

Acknowledgments 32

References 33

Appendix 34

1 Introduction

This project was funded by Miljömålsrådet through the Swedish Radiation Protection Authority (SSI) in order to calculate hourly values of CIE-weighted UV-radiation and global radiation for 1980-2000 over northwest Europe. To have access to long series of data covering large areas are essential to be able to track changes in the environment and to evaluate eventual effects. In this case the most obvious connection to existing environmental goals is to “Reduced climate impact”, “A safe radiation environment” and “A protective ozone layer”. In these cases, data can be used to calculate the carbon uptake and emission, direct data on long-term UV-trends and to enable an extended analysis between changes in the UV and the incidence of skin cancer. But, the produced data set can also be used for other purposes and studies, such as algae blooming.

An already existing model system, STRÅNG, does create these kinds of information together with more radiation parameters. The development of STRÅNG (Landelius et al., 2001), was funded by the Swedish Environment Agency, the Swedish Meteorological and Hydrological Institute and the Swedish Radiation Protection Authority (1998-2001). The hourly information are free available for non-commercial use at www.smhi.se/strang, at this website data can be retrieved both as time series, charts and fields from 1999 up to today.

The STRÅNG-model system is based on information from an operational 2-dimensional mesoscale analysis system at SMHI, called the MESAN-model (Häggmark et al., 2000). This model combines information from ground based observations, satellites, radar and from numerical weather prediction (NWP) models. The outputs are different meteorological parameters on an 11x11 km (earlier 22x22 km) resolution for every hour. The MESAN data is only available from 1998 to today. So, to calculate CIE-weighted UV-radiation and global radiation for the period 1980-2000 has to be done in another way. This report describes the procedure to calculate this data, which input data that has been used and also validation of the outputs.

The results of this project are available and can be downloaded from www.smhi.se/strang/omna.

2 Background

To be able to detect trends in the atmosphere, comparisons between past and present climate is a hot topic today. In this kind of studies it is of great importance to use homogeneous data. But, this is not as trivial as it might be assumed, it is instead a very difficult task, especially if the homogenous data shall cover a large geographical area with high spatial and temporal resolution.

The constant development of measurement techniques, remote sensing and atmospheric modelling are the main reasons why it is so difficult to retrieve homogenous data for long time periods. This problem exists for all kinds of atmospheric variables, not only for radiation parameters that this project is focused on.

To try to solve this problem, several meteorological institutes are working in different kinds of re-analysis projects. The main objectives in re-analyses are to create reasonably homogeneous data that covers many years in time and over a large spatial area, the whole globe or for example Europe, with one and the same model for the whole period.

A comprehensive re-analysis data set originates from the European Centre for Medium-Range Weather Forecasts (ECMWF) and is called the ERA-40 data set (Uppala et al., 2005). The ERA-40 data set cover the period September 1957 to August 2002 and covers the whole globe with a spatial resolution of about 125 km. The data set is also represented in 60 vertical levels above the ground. The data set includes both analyses and forecasts. All ERA-40 analyses are made every 6 hour and includes data assimilation, which means that for example observations and satellite data are all weighted together to achieve the best possible analysis of the atmosphere.

Today, several other European projects are just in their starting blocks to model a more high resolution re-analysis over Europe, but no final results are available.

Another way to achieve high resolution gridded data for many years is to downscale global re-analyses such as the ERA-40 data set. Then a 3-dimensional model is used over a limited geographical area with boundaries from the global re-analysis, i.e. the re-analysis is forced in to the downscaling model through the boundaries. In that way a much higher, both spatial and temporal, resolution can be achieved. The drawback is instead that most of this kind of models does not include any data assimilation, the only information about the atmosphere is forced in to the model through the boundaries.

Concerning radiation parameters, cloudiness plays an important role to the analyses. In 3-dimensional NWP models and re-analysis models there is today no developed technique to assimilate the cloudiness from satellite data in to the model. But of course there are projects working with these problems today.

There is on the other hand a 2-dimensional technique developed to assimilate the cloudiness from satellites, such a model has been developed and well used at SMHI, the model is called MESAN and is used operationally at SMHI since 1998 (Häggmark et al., 2000). The model produces 2-dimensional fields over northwest Europe with a spatial resolution of 11x11 km (earlier 22x22 km) for each hour for the parameters, temperature, maximum- and minimum-temperature, wind, gust, visibility, relative humidity, pressure, precipitation, fresh snow, total cloud amount, amount of low clouds, cloud base and cloud top and so on. The analyses are created from a first guess field, a

NWP forecast, which is getting modified by regular and irregular distributed information from satellites, radar and ground based observations. Since the model has gone through several development projects during the years, the MESAN data are not homogenous in time. This is also caused by developments in the NWP model that is used as first guess field in MESAN. Also the satellite and radar data used in the model have gone through improvements. The same is also valid for ground based observations, here several manual stations have been replaced by automatic stations, some stations have stopped, and new stations have started, so to find homogenous data is very difficult.

3 Data sources

To be able to model radiation for the period 1980 to 2000 we need to find relevant input data for this period. One demand is homogeneity (stability over time and space), another one is good spatial and temporal resolution. Also needed is that the geographical extent includes northwest Europe.

This chapter describes the model data that has been used in this project. Also descriptions of all observations that have been used are made in this chapter. The observations have been used both for development of the model technique and for validation.

3.1 ERA-40

ERA-40 is a comprehensive set of global re-analyses from September 1957 to August 2002 (Uppala et al., 2005). The re-analyses have been performed by the European Centre for Medium-Range Weather Forecasts (ECMWF) in Reading, United Kingdom (www.ecmwf.int). The re-analyses are archived in ECMWF's Meteorological Archive and Retrieval System (MARS) (Kållberg et al., 2004) where registered users from the member states can select and retrieve global re-analyses. The atmospheric model used for ERA-40 has 60 levels in the vertical, T159 spherical-harmonic representation for basic dynamical fields and a reduced Gaussian grid with approximately 125 km spacing for surface and other grid points fields. ERA-40 includes four analyses per day (00, 06, 12 and 18 UTC). The forecasts are based on the 00 and 12 UTC analyses and are stored in 3 hour intervals from 00 to 72 hours and in 6 hour intervals from 72 to 240 hours.

Observations used in ERA-40 include both observations from the operational ECMWF archives and data supplied to ECMWF by external institutions for use in the re-analysis. The input data to the ERA-40 re-analyses originates from the following sources.

1) SYNOP/SHIP, land and ship synoptic observations
2) Radiosondes
3) Pilot balloons
4) Aircraft
5) Buoys
6) Satellite radiances
7) Satellite winds
8) Scatterometer
9) PAOBs (Pseudo Surface Pressure Observations)

The total ozone data in ERA-40 originates from the satellite based instruments, TOMS (Total Ozone Mapping Spectrometer) where the total column ozone is available and from the SBUV (Solar Backscatter UltraViolet) where layer ozone is available from 1979 to 1988 and from 1991 to 2000. However, during several periods, notably during 1995 and 1996, TOMS data have not been used in the ERA-40 model.

3.2 The Rossby Centre regional atmospheric climate model

The Rossby Centre regional atmospheric climate model, RCA, is a 3-dimensional downscaling model developed and used at SMHI. The model is based on the operational regional NWP model HIRLAM (Undén et al., 2002) but with process formulations and parameterizations adjusted to suit long-term climate simulations (Rummukainen et al., 1998). In this project the new version of the Rossby Centre regional atmospheric climate model (RCA3) has been used (Kjällström et al., 2005). The RCA3 model is mainly used for simulate climate scenarios for the future and was also used as basis for the "Climate and Vulnerability investigation" that was ordered by the Swedish government. The aim of the investigation was to discover future problems for the community regarding climate changes. For those simulations the spatial resolution was 50x50 km and the temporal resolution 30 minutes. In this study, the Rossby Centre at SMHI has instead provided the project with RCA3 hourly analyses on a 22x22 km grid on the area shown in Figure 3.1, black rectangle. ERA-40 data has been used at the lateral boundaries. To avoid strange features near the lateral boundaries the model area is bigger then needed. The area of interest in this project has been cut out from the model domain (see Figure 3.1, red rectangle). The used model domain in this project is the same as in the STRÅNG-system.

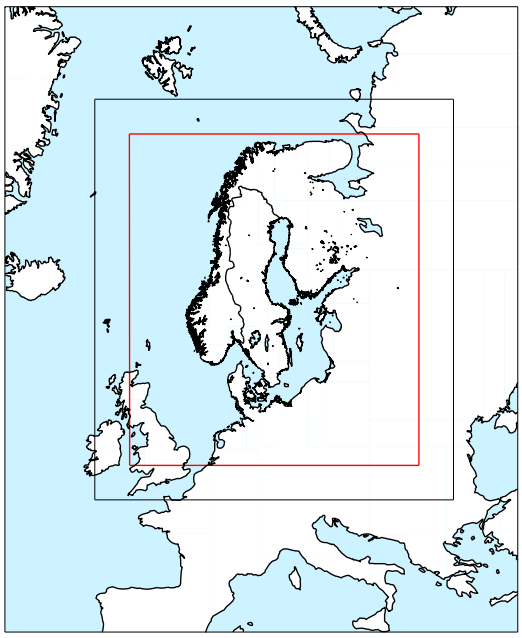

Figure 3.1: The black rectangle corresponds to the model domain in RCA3 that has been used in this project and the red rectangle has been cut out and used as model domain in the creation of CIE-weighted UV-radiation and global radiation.

3.3 Observations

3.3.1 Ozone

Available ozone measurements in the model domain are the stations listed in Table 3.1, also available years during the period 1980-2000 are listed. Since the ozone variation is relatively slow, observations are only given once a day.

Table 3.1: List of stations with total ozone measurements used in this project.

Station, country	Latitude	Longitude	Available years
Bergen, Norway	60.38º N	5.33º E	1980-2000 (missing 1994-1996)
Potsdam, Germany	52.36º N	13.07º E	1980-2000
Belsk, Poland	52.00º N	21.00º E	1980-2000
Hradec Králové, C. R.	50.15º N	15.14º E	1980-2000
Norrköping, Sweden	58.58º N	16.15º E	1983-2000

3.3.2 UV-radiation

All UV in this report refers to CIE-weighted UV-radiation, which is obtained by weighting spectral UV-radiation by the action spectrum for erythema (McKinley and Diffey, 1987). The used hourly UV-radiation measurements are listed in Table 3.2.

Table 3.2: List of stations with hourly UV-radiation measurements used in this project.

Station, country	Latitude	Longitude	Available years
Landvik, Norway	58.34º N	8.60º E	1996-2000
Blindern, Norway	59.64º N	10.72º E	1995-2000
Kise, Norway	60.77º N	10.81º E	1997-2000
Trondheim, Norway	63.42º N	10.41º E	1999-2000
Tromsö, Norway	69.68º N	18.97º E	1996-1999
Østerås, Norway	59.95º N	10.60º E	1999-2000
Norrköping, Sweden	58.58º N	16.15º E	1993-2000

UV-measurements often includes an offset, which means that during night time the logger also register UV-radiation, which is wrong, about 0.01 mWh/m². Later on, all observations are corrected for this offset before they are used. This had not been done at the observations from Norway, therefore it has been done in this project before they were further used. Also, from the Swedish station it is noted if an observation is measured or interpolated, in case of for example technical problems. To minimize the uncertainty for the future usage of the observations, interpolated observations are not used.

3.3.3 Global radiation

The global radiation measurements that have been used originate from the 12 Swedish radiation stations listed in Table 3.3. As for the Swedish UV-measurements, if a short time period is missing, because of for example, technical problems, the observed values are interpolated, and notified in the observation archive, such interpolated observations have not been used in this project, only measured values have been used to minimize the uncertainty in the future validation.

Table 3.3: List of stations used in this project with global radiation measurements together with the available years.

Station	Latitude	Longitude	Available years
Kiruna	67.83º N	20.43º E	1983-2000
Gunnarn	64.96º N	17.70º E	1983-1986
Luleå	65.55º N	22.13º E	1983-2000
Umeå	63.82º N	20.25º E	1983-2000
Östersund	60.48º N	14.50º E	1983-2000
Borlänge	63.20º N	15.43º E	1987-2000
Karlstad	59.37º N	13.47º E	1983-2000
Stockholm	59.35º N	18.07º E	1983-2000
Norrköping	58.58º N	16.15º E	1983-2000
Göteborg	57.70º N	12.00º E	1983-2000
Visby	57.67º N	18.35º E	1983-2000
Växjö	56.93º N	14.73º E	1983-2000
Lund	55.72º N	13.22º E	1983-2000

4 Calculation of CIE-weighted UV-radiation

The approach to calculate CIE-weighted UV-radiation (later on referred to only UV) has been done in two steps: step number one, to calculate the UV for a clear sky, and step number two to reduce the clear sky radiation with a cloud modification model. The second step can be done in several ways. Mainly three ways have been considered and tested in this project. All calculations, both for clear and cloudiness sky have been done on the area shown in Figure 3.1, red rectangle. Both for estimation of the cloud modification model and in the validation for hourly values only observations when the sun height is above or equal to 25º have been used. In this way problems of existing small errors in both quantities as well as problems to model UV at low solar altitudes which strongly might influence the cloud modification model, is reduced.

In the validation for UV and also for global radiation in Chapter 5 the error of an individual value is:

$$\varepsilon = UV_m - UV_o \tag{1}$$

The subscripts *m* and *o* refers to the modelled and observed UV or global radiation. Having a set of *N* hourly, daily, monthly or yearly ε-values different error quantities can be calculated. In this project three error quantities have been used, namely:
The mean bias deviation (MBD);

$$MBD = \left(\sum_{i=1}^{N} \varepsilon \Big/ N \right) \tag{2}$$

the mean absolute deviation (MAD);

$$MAD = \left(\sum_{i=1}^{N} |\varepsilon| \Big/ N \right) \tag{3}$$

and the root mean square deviation (RMSD);

$$RMSD = \sqrt{\left(\sum_{i=1}^{N} \varepsilon^2 / N \right)} \tag{4}$$

Note that the deviation is used instead of error because the observations are not a perfect reference.

4.1 Clear sky model

All input data used in the clear sky model are retrieved on a 22x22 km spatial resolution for the area shown in Figure 3.1, red rectangle. All input fields are also stored in the same coordinate system, in this case a rotated latitude longitude coordinate system, often used in atmospheric models for Europe. In this case with the South Pole at 10° E and 30° S. Each input field includes 102 grid points in west-east direction and 116 grid points in south-north direction, totally 11832 number of grid points. Of course, also the results from the clear sky model have the same geographical extent, spatial resolution and coordinate system as the input fields.

For creation of the clear sky UV the Fast and easy UV simulation tool (FastRT) (Engelsen and Kylling, 2005) has been used. This model is only developed for point calculations, and not for a whole model domain that is needed in this project. As this would be rather time consuming the FastRT model has been used to create a “lookup table”, which includes all needed input data.

Afterwards each input field, for example ozone, albedo and sun height together with the “lookup table” have been used as input to a multi-dimensional spline interpolation. In that way one field for the whole model domain for clear sky UV can be computed for every hour.

4.1.1 Input data

The needed parameters to compute the clear sky UV in the FastRT model are listed in Chapters 4.1.1.1-4.1.1.4.

4.1.1.1 The solar zenith angle

The solar zenith angle calculation is based on the Kepler’s equation. The input parameters are the corresponding latitude and longitude for each grid point in the model domain, together with the time in UTC given in year, month, day, hour and minute.

4.1.1.2 Altitude and surface albedo

The altitude, i.e. the topography is the same altitude as the one used in the RCA3 model, described in Chapter 3.2. Also the surface albedo originates from the RCA3 model and is calculated once a day and is valid for global radiation. A small correction has been done before any further usage of the albedo for the UV. An example of the surface

albedo at 12 UTC on the 1st of January 1980 is shown in the left panel of Figure 4.1. In the right panel instead the altitude is shown.

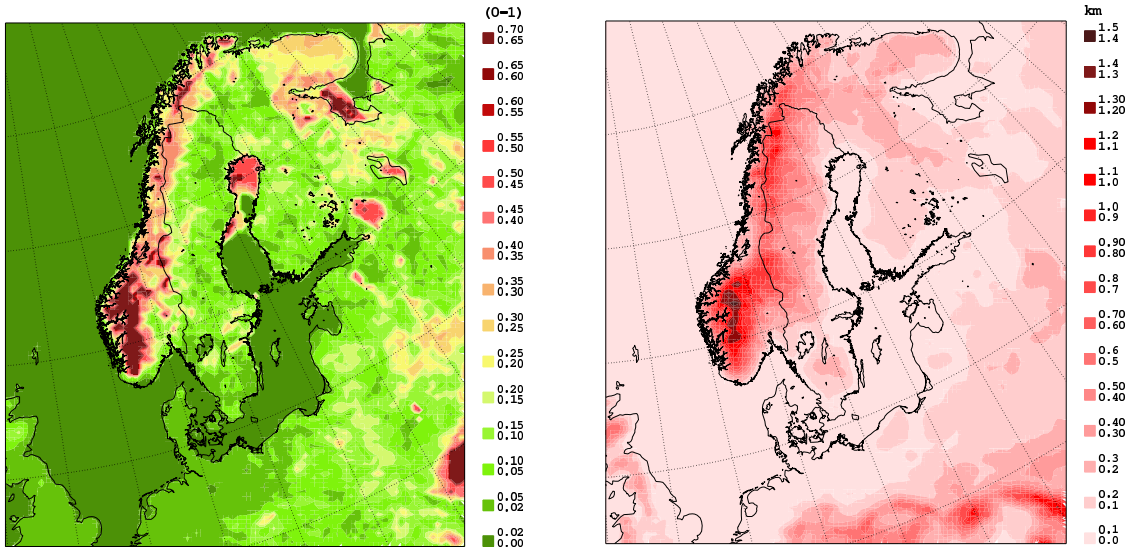

Figure 4.1: Left: The surface albedo field at 12 UTC at the 1st of January 1980 from RCA3. Right: The altitude field.

4.1.1.3 Aerosols

The aerosols in the atmosphere can both absorb and scatter radiation, both the amount and the aerosol size plays an important role. However, there are very few routine observations done of the aerosols optical characteristics. The information needed in this project is not at present available. Therefore, we have used aerosol optical depth (AOD) data observed in Norrköping (Carlund et al., 2003), combined with older courser measurements to model the long-term yearly and seasonal variation of the Ångström turbidity. There is also a latitude dependent factor in the model.

The sometimes very large day to day variation has not been possible to model. Hopefully, the eventual long-term trend caused by aerosols will be taken care of.

The Ångström turbidity, β, is one parameter in the equation $AOD_\lambda = \beta \lambda^{-\alpha}$, where λ is the wavelength of the radiation, α is an aerosol size dependent parameter (here set to 1.3) and β is the Ångström turbidity when λ is 1 µm.

An example of the Ångström turbidity coefficient used as input to the clear sky model for latitude 60° N during 1980-2000 is shown in Figure 4.2, left. The two peaks found close to 1983 and 1993 are caused by the volcano eruptions of El Chichon and Pinatubo. Otherwise the turbidity coefficient has it maximum during summertime and minimum in wintertime.

4.1.1.4 Total ozone

The total ozone has been retrieved from the ERA-40 archive. Figure 4.2, right shows an example of the total ozone field from ERA-40 at the 1st of July 2000. To discover and adjust possible systematic errors in the ERA-40 total ozone analyses a very rough and simple method has been used. The data have been compared against the ozone

measurements listed in Table 3.1. Since most of the UV is located around noon the 12 UTC ERA-40 analyses are used. The quota between the ERA-40 analysis and the observed ozone is plotted in Figure 4.3 (black dots). As seen some peaks exist especially around year 1990, here the ERA-40 ozone is much higher then the observed ozone amount. The peaks for the years 1988-1991 depends on the missing TOMS and SBUV satellite data in the ERA-40 data assimilation, the peaks after 1991, especially during 1995 and 1996 is caused by missing data from the TOMS satellites (see Chapter 3.1). Since this is valid for the whole model domain it is appropriate to make a correction for this based on the observations in Table 3.1. The correction factor has been calculated as the mean value for all quotas per day. This daily factor has then been applied on the ozone field from the ERA-40 analysis before it is further used in this project. The quotas using the adjusted total ozone can also be seen in Figure 4.3, (red dots) and it is evident that the peaks are strongly reduced. The gaps in Figure 4.3 indicate missing observations.

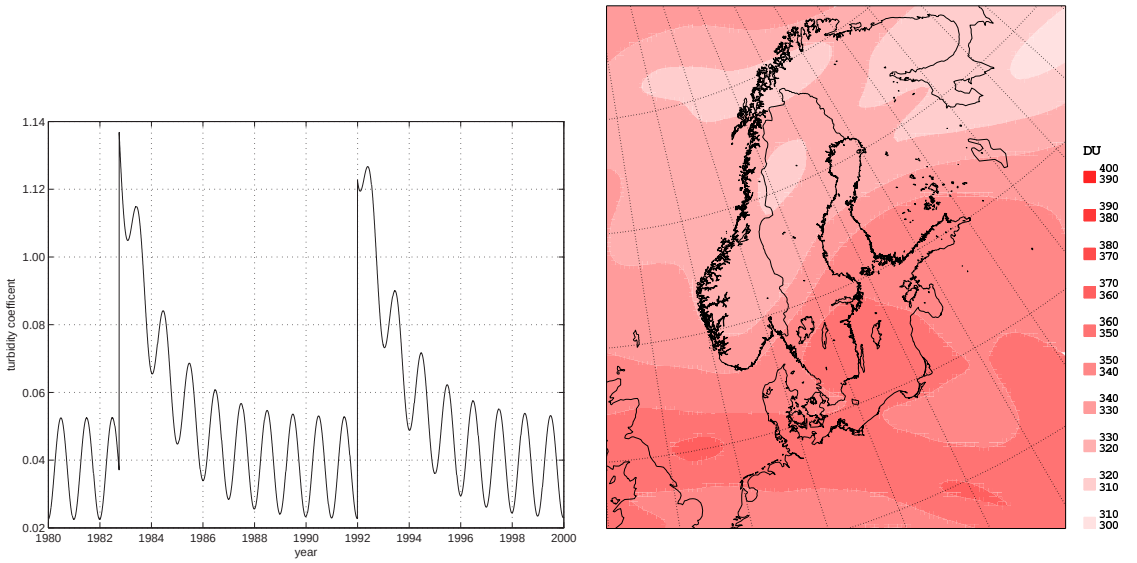

Figure 4.2: Left: The graph illustrates how the Ångström turbidity coefficient changes in the model during 1980-2000 for latitude 60º N, the two peaks close to 1983 and 1993 were caused by volcanic eruptions. Right: Total ozone from ERA-40 at 12 UTC the 1st of July 2000.

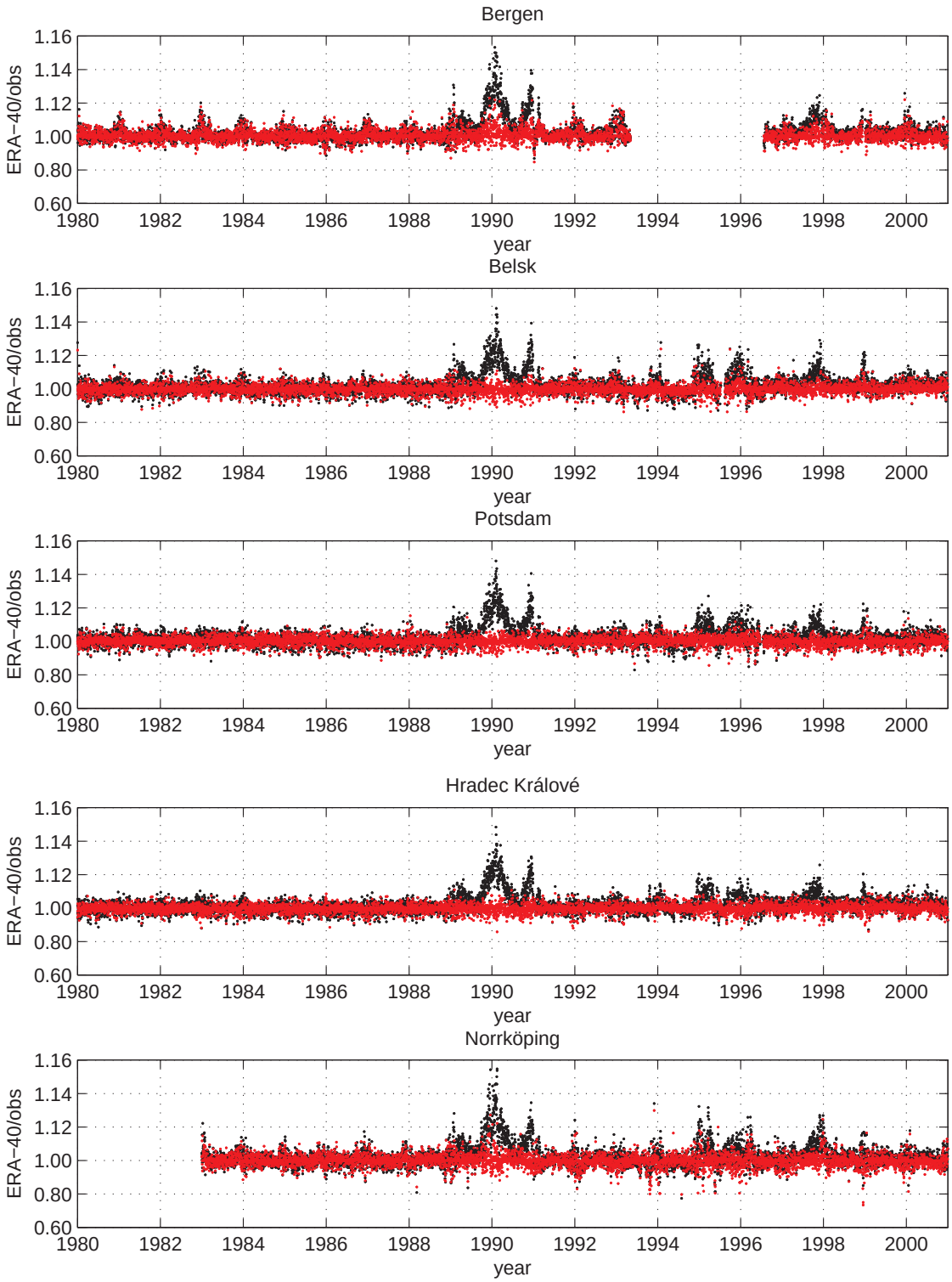

Figure 4.3: The black dots correspond to the total ozone quota between ERA-40 and observed values from Bergen, Belsk, Potsdam, Hradec Králové and Norrköping. The red dots correspond instead to the corrected ozone quota between ERA-40 and observations from Bergen, Belsk, Potsdam, Hradec Králové and Norrköping.

Also a scatter plot for the corrected ERA-40 ozone analyses against the observed ozone from the stations listed in Table 3.1 is illustrated in Figure 4.4. The ozone errors are calculated in the same way as for UV (Equation 1-4) this gives that the ozone data is free of bias, the MAD is 2% and the RMSD is 3%.

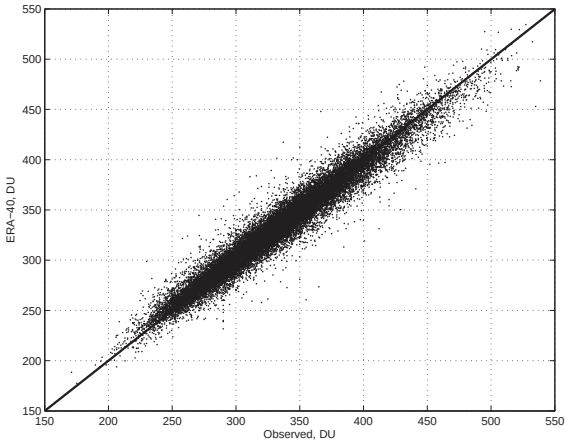

Figure 4.4: Scatter plots for the corrected ozone analyses from ERA-40 versus the ozone measurements listed in Table 3.1.

4.1.2 Results

The "lookup table" was made with a set of intervals and steps for each needed input parameter. The intervals and steps for all input parameters are listed in Table 4.1. The interval has been chosen as maximum and minimum of all input data for each hour during 1980-2000. The steps have been chosen and tested dependent of the matter of influence to the UV. But also the computer time to calculate all clear sky analyses has been considered.

Table 4.1: All input parameters with corresponding interval and step that have been used to create a "lookup table" in order to model the clear sky UV.

Parameter	**Interval**	**Step**
Turbidity coefficient	0.01-0.17	0.02
Albedo	0-0.7	0.05
Altitude	0-1.5 km	0.3 km
Ozone	160-480 DU	10 DU
Solar zenith angle	20-90º	1º

With this "lookup table" together with each ozone, albedo and altitude field it is possible to model the clear sky UV for the whole model domain. The Ångström turbidity coefficient and the solar zenith angle is instead of being an input field to the model a subroutine in the model itself and is calculated for each hour and each grid point.

The output from the clear sky model is one field of clear sky UV per hour for the years 1980-2000. As an example the clear sky UV at 12 UTC for the 1st of July 2000 is illustrated in Figure 4.5.

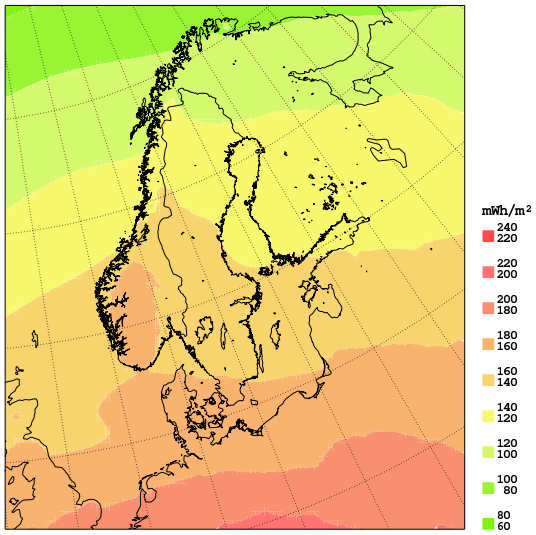

Figure 4.5: Hourly clear sky UV for 12 UTC at the 1st of July 2000.

For validation of the modelled clear sky UV, the cloud fraction alternatively the sunshine duration is needed from the same place as the UV-measurements are made. This information is presently only available from one UV-measurement site listed in Table 3.2, namely Norrköping, Sweden, where the sunshine duration is available. The clear sky outputs have been validated against the clear sky UV-observations in Norrköping for the years 1993-2000. The observed clear sky is defined as when the sunshine duration is one hour per hour. This gives totally 3347 samples.

In the left panel in Figure 4.6 the modelled UV against the observed UV is plotted. Here, it can be noticed that the modelled UV indicates a systematically higher value then the observed UV. With the assumption that the modelled clear sky UV in Norrköping is representative for the whole model domain, a clear sky correction can be done to overcome the systematic higher modelled UV. Therefore, the modelled clear sky UV has been corrected as in Equation 5, where *N* is total amount of clear sky samples. The equation gives a correction factor of 0.95, i.e., the clear sky UV is about 5% to high, the corrected modelled clear sky UV versus observations is illustrated in the right panel in Figure 4.6. The correction have also been tested for all stations listed in Table 3.2, and the assumption that Norrköping is representative for the whole model domain seems to hold even for the rest of the stations.

$$UV(corr)_m = UV_m \cdot \frac{\sum_{i=1}^{N} UV_{oi}}{\sum_{i=1}^{N} UV_{mi}} \qquad (5)$$

In the corrected modelled clear sky UV no bias exists, the MAD is on the other hand 4.8% and the RMSD is 6.8%. The error is probably caused by the variation in the aerosols and albedo that have not been possible to include in the model, also the fact that the observations is representative for one point and in the model for an area, 22x22 km, influence on the result.

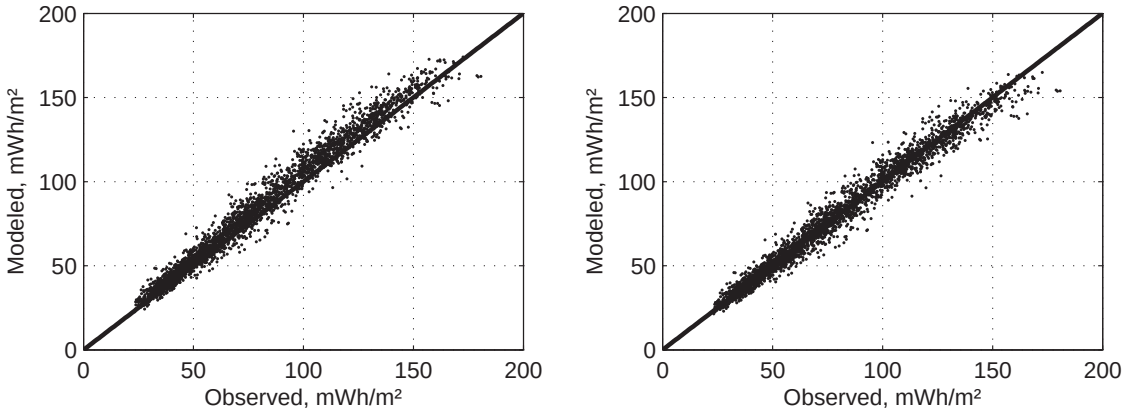

Figure 4.6: Scatter plots for hourly modelled UV versus observed UV for clear sky (one hour sunshine duration per hour) for Norrköping 1993-2000. Left: Original modelled clear sky UV versus observed clear sky UV. Right: Corrected modelled clear sky UV versus observed clear sky UV. The straight line in both panels corresponds to the 1:1 line.

4.2 Development of a cloud modification model

Having a clear sky model for the UV it is now necessary to develop a model that can be applied for any sky condition based on available information. Using measured data in combination with the total cloudiness and the cloud water content from the RCA3 model it is possible to study how clouds modify the modelled clear sky values. The result will be a cloud modification model, CMM.

To avoid that the same observations are used both to estimate a CMM and to validate the outputs from the CMM, the hourly data has been separated in a chance generator. All UV-measurements that have been used for estimation of the CMM and for validation are listed in Table 3.2. For the same observation sites the modelled clear sky UV, the total cloudiness and the cloud water content from the RCA3 model have been retrieved.

In the following, the ratio between observed UV(E) and modelled clear sky UV(E_0) will be used. To avoid problems taking the ratio between small values, which are strongly affected by uncertainties, only UV when the sun height is above or equal to 25º is used. With this data set it is possible to study the E/E_0 ratio as a function of the cloud parameters from RCA3 (total cloudiness and cloud water content). This data set includes totally 49901 samples, where 50% have been used to estimate the CMM and 50% to validate the outputs from the CMM, i.e. the modelled UV for all sky conditions.

For estimation of a CMM, different tests have been carried out, all tests are dependent on either the total cloudiness or the cloud water content. Some tests have also included 2-dimenional dependencies for example the E/E_0 ratio as a function of both the total cloudiness and the sun height. For hourly E/E_0 ratios a large scatter exists, therefore the median and mean values of the E/E_0 ratio in different cloud and sun height intervals have been used instead. In general when this kind of method is applied it is important that the number of samples in each interval is not too small, otherwise the median and mean values will not be representative for the interval and might cause errors in the CMM outputs.

For the validation of the different CMM outputs, the cases of high UV have been considered as the most important ones, since the damaging effects of UV is most pronounced when the sun is high and the sky is relatively clear.

Also for all tests the E/E_0 ratio for clear sky have been forced through $E/E_0 = 1$. In that way, the clear sky UV is not reduced because of the scatter in the hourly values.

The tests that have been carried out to find the most appropriate CMM are:

1) E/E_0 as a function of the total cloudiness.
2) E/E_0 as a function of the cloud water content.
3) E/E_0 as a function of the total cloudiness by minimization of the error.

1) E/E_0 as a function of the total cloudiness.
In this test the median and mean values of E/E_0 in 19 intervals of the total cloudiness have been calculated. In this calculation the end points are not represented, i.e., clear and overcast sky. When the CMM later on is applied on the validation data it is important that the end points are represented otherwise the interpolation routine might crash. Therefore, the E/E_0 ratio for clear and overcast sky has to be added. For clear sky the E/E_0 ratio is set to one (so that the clear sky UV not is reduced) and for overcast sky the median respectively the mean values of E/E_0 have been calculated. This is illustrated in Figure 4.7, left, the black dots corresponds to all samples of E/E_0 versus the total cloudiness, the red and blue dots to the median and mean values of E/E_0 calculated in 21 intervals of the total cloudiness. With these median and mean values, together with the total cloudiness and clear sky UV, it is now possible to model the UV for any sky condition with a 1-dimensional spline interpolation.

2) E/E_0 as a function of the cloud water contents.
Here, the same procedure as in test number one is applied, but instead of the total cloudiness from the RCA3 model, the cloud water content has been used. Also here the end points, clear and overcast sky has to be added to the original median and mean values of E/E_0. Different in this test is also the numbers of interval the median and mean values of E/E_0 have been calculated in. In this test 39 intervals have been used since the cloud water content vary from 0-2(3) g/m^3. The E/E_0 ratio versus the cloud water content is plotted in Figure 4.7, right. The red and blue dots in the figure corresponds to the median and mean values of E/E_0 versus the cloud water contents calculated in 41 intervals. With this information it is now possible to model the UV for any sky condition with the cloud water content and clear sky UV as input in a 1-dimensional spline interpolation.

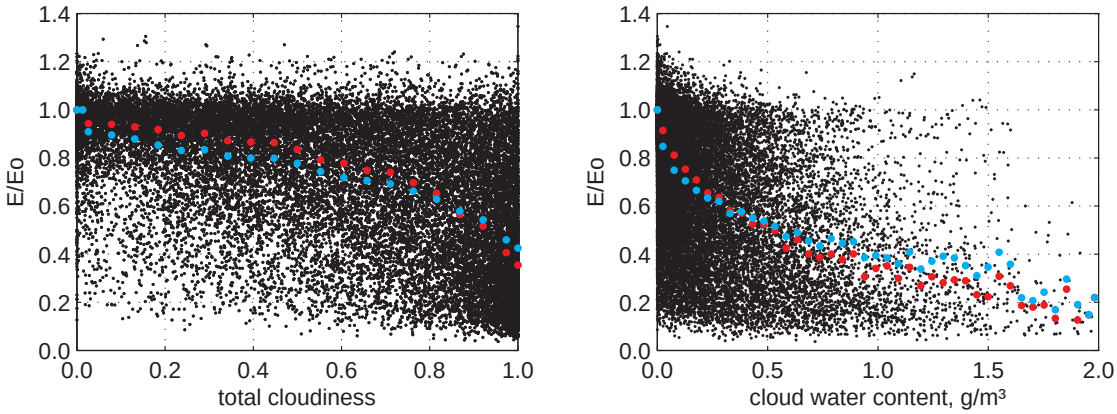

Figure 4.7: Left: The E/E_0 ratio is here plotted against the total cloudiness from the RCA3 model (black dots). The red and blue dots correspond to the median and the mean values calculated in 19 intervals plus the E/E_0 ratios for clear (set to 1) and overcast sky (median and mean values of E/E_0 when the total cloudiness is equal to 1 at the x-axes). Right: The E/E_0 ratio is here plotted against the cloud water content from the RCA3 model (black dots). The red and blue dots are calculated in the same way as for the left panel, but here 39 intervals are used instead.

3) E/E_0 as a function of the total cloudiness by minimization of the error.
In this test a function as Equation 6 has been applied (Kasten and Czeplak, 1980).

$$t(C_T) = 1 - (1 - t(1)) \cdot C_T^{\alpha} \qquad (6)$$

Here C_T is the total cloudiness, and t the function dependent on the total cloudiness (C_T), $t(1)$ is the estimated cloud effect for overcast sky and α is a coefficient that also has to be estimated from the data set (the E/E_0 ratio and the total cloudiness).

As in test number 1 the same median and mean values of E/E_0 in the 19 intervals of the total cloudiness have been used. But in this test more samples are needed in the minimization routine, therefore all samples inside the median and mean values ± one standard deviation of E/E_0 have been used to estimate $t(1)$ and α in Equation 6. Figure 4.8, left, illustrate the function in Equation 6 applied on all values of E/E_0 inside the median values ± one standard deviation. The right panel in Figure 4.8 illustrates instead the function applied on all values of E/E_0 inside the mean values ± one standard deviation. These functions have then been applied on all clear sky UV with the total cloudiness from the RCA3 model as input.

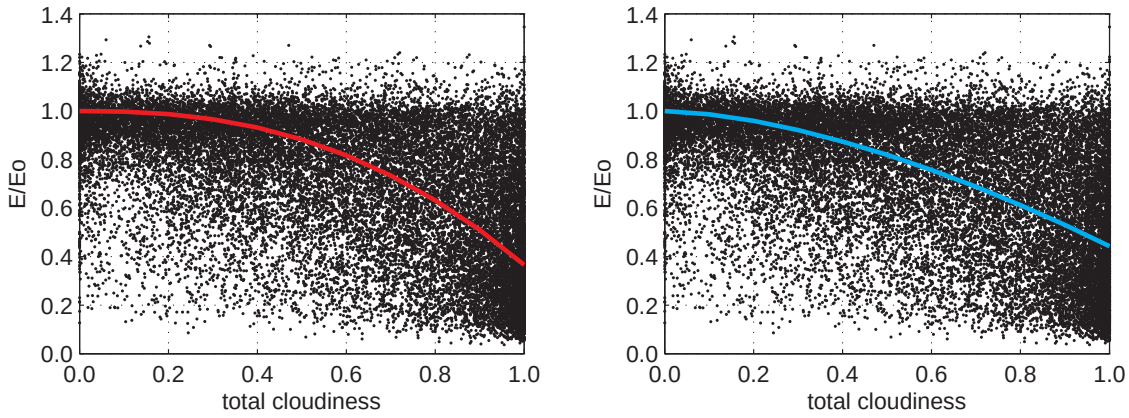

Figure 4.8: The black dots correspond to the ratio E/E_0 plotted as a function of the total cloudiness. Left: The red curve corresponds to the function applied on the samples inside the median values of E/E_0 ± one standard deviation calculated in 19 intervals for the total cloudiness. Right: The blue curve corresponds instead to the function applied on the samples inside the mean values of E/E_0 ± one standard deviation calculated in 19 intervals of the total cloudiness.

The CMMs in the three different tests has now been applied on the validation data, i.e. the data is independent from the data used in the estimation of the CMMs. Both median and mean values of the E/E_0 ratio have been used in the three tests. The hourly statistics of the modelled UV for all tested CMMs is listed in Table 4.2.

Table 4.2: List of all error quantities calculated for hourly UV values modelled with the CMMs in test number 1-3, when both the median and mean values of the E/E_0 ratio have been used.

	Test 1		**Test 2**		**Test 3**	
	Median	**Mean**	**Median**	**Mean**	**Median**	**Mean**
MBD	+3.8%	+0.6%	+5.3%	+2.1%	+7.2%	+5.3%
MAD	26.3%	27.0%	27.3%	27.6%	27.2%	26.8%
RMSD	37.3%	36.7%	38.5%	37.7%	39.1%	37.7%

For validation of the results when the different CMMs have been used, we first focus on test number 1 and 2 since the same method have been used to estimate the CMMs. From Table 4.2 it can be noticed that for test number 1 and 2 the MBD and RMSD indicates that it is better to use the mean values of the E/E_0 ratio when the CMM is estimated, especially when the total cloudiness are used (test number 1). Scatter plots for test number 1 show that this is a false signal, see Figure 4.9, left and right. When the mean values of E/E_0 are used (Figure 4.9, right) the overestimation of low UV amounts is getting compensated by the underestimation of high UV amounts. If such a CMM should be used the clear sky UV, that is most important in this project, will not be preserved. Also when the median values of E/E_0 are used in test number 1, the clear sky UV are not preserved (Figure 4.9, left), but it is still better preserved then when the mean values are used (Figure 4.9, right).

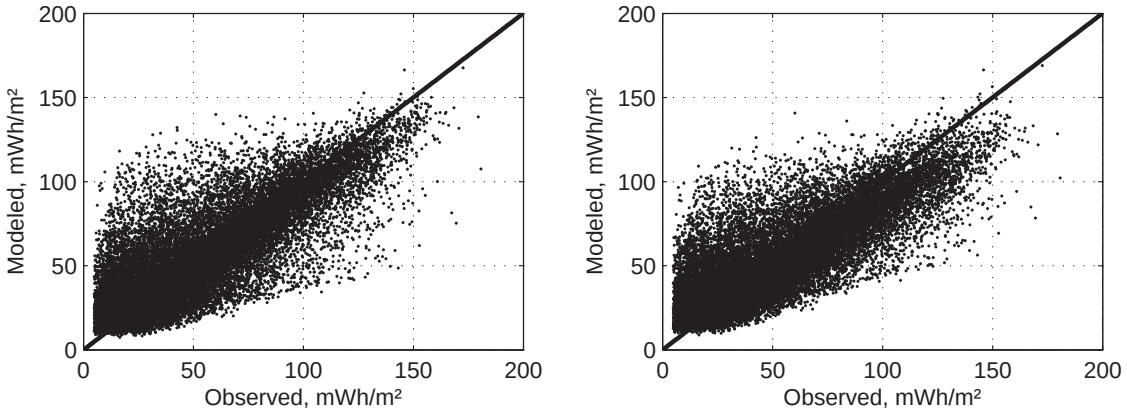

Figure 4.9: Scatter plots for modelled UV when the CMM in test number 1 has been used versus observed UV from the independent observations. The left panel corresponds to the modelled data when median values of the E/E_0 ratio have been used. The right panel corresponds instead to the modelled data when the mean values of the E/E_0 ratio have been used in the CMM.

For test number 3, the clear sky UV is better preserved, since the function (Equation 6) is forced through E/E_0 for clear sky, this was also the case for test number 1 and 2, but here even the high UV when only small amounts of clouds exist in the model will be preserved, see Figure 4.10.

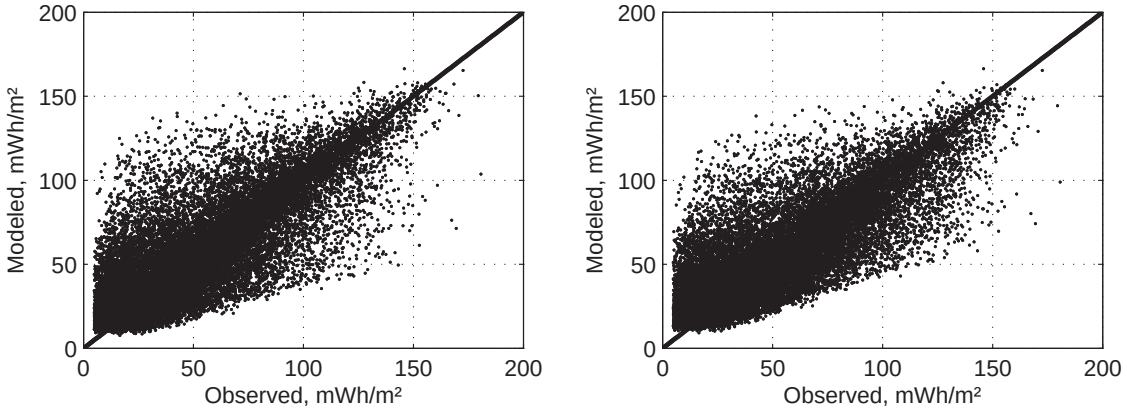

Figure 4.10: Scatter plots for modelled UV when the CMM in test number 3 has been used versus observed UV from the independent observations. The left panel corresponds to the modelled data when median values ± one standard deviation of the E/E_0 ratio have been used in the estimation of the CMM and the right panel when mean values ± one standard deviation of the E/E_0 ratio have been used instead.

From the scatter plots for test number 1 (Figure 4.9) and test number 3 (Figure 4.10) it is very clear that test number 3 have to be used in the future despite the results listed in Table 4.2. If the CMM in test number 3 estimated from the median or mean value ± one standard deviation of the E/E_0 ratio should be used is difficult to say from a look at the scatter plots. The errors listed in Table 4.2 on the other hand shows that the best statistics are found when the estimation of the CMM were build on the mean values of E/E_0 ± one standard deviation. But even in this case (Figure 4.10, right) the low UV amounts are overestimated (+5.3%), but the most important UV are preserved, i.e., the

high UV amounts. The overestimation of low UV values is caused by an overestimation of the cloud effect (*t(1)* in Equation 6) for overcast sky. As seen in Figure 4.7 and 4.8 the largest scatter of E/E_0 exists for large cloud amounts, especially above the median and mean value of E/E_0. These cases, when the real world has clear sky and the model has overcast sky are very difficult to model correct independent of the CMM. Instead the samples increases the standard deviation and influence the estimation of the cloud effect for overcast sky (*t(1)*) in a negative matter, i.e., the cloud effect is getting to high for overcast skies. Trying to eliminate some of the bias in the data set, tests have been done where the outliers not are a part of the minimization routine. By using the data inside the mean value of the E/E_0 ratio ± one standard deviation, instead the samples inside the mean value of E/E_0 - one standard deviation and mean value of E/E_0 + a half standard deviation for overcast and almost overcast skies have been used, for lower cloud amounts the same samples have been used as earlier. In this way the cloud effect for overcast sky is reduced from 0.4426 to 0.3856. When this CMM, with the lower cloud effect for overcast skies, is applied on the validation data the bias has been reduced from +5.3% to +3.4%, the other error quantities is influenced very little, +0.1% for the MAD and +0.3% for the RMSD, therefore this CMM will be used in the future. The differences between the old and new CMM in test number 3 where the mean values of E/E_0 ± one standard deviation have been used and when instead the mean values of E/E_0 instead only are calculated in the interval mean value – one standard deviation to mean value + a half standard deviation for overcast skies is illustrated in Figure 4.11.

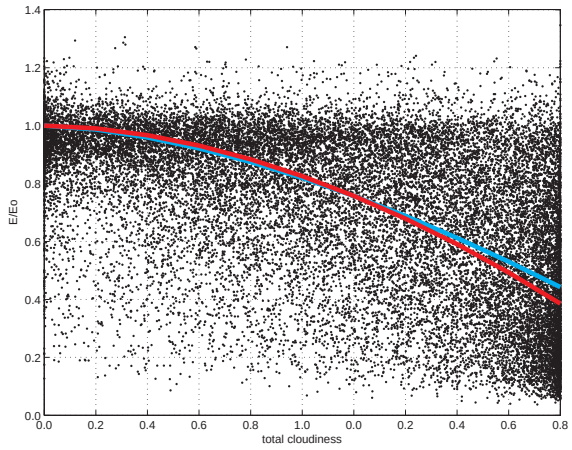

Figure 4.11: The black dots correspond to the ratio E/E_0 plotted as a function of the total cloudiness. The blue curve corresponds to the function applied on the samples inside the mean values of E/E_0 ± one standard deviation calculated in 19 intervals for the total cloudiness. The red curve corresponds instead to the function applied on the samples inside the mean values of E/E_0 - one standard to the mean value + a half standard deviation calculated in 19 intervals for the total cloudiness.

Also tests where the CMM has been dependent on both total cloudiness and cloud water content and total cloudiness together with the sun height have been performed. When the CMM has a 2-dimensional dependencies the median and mean values of the E/E_0 ratios have been used in the same way as earlier, but here the median and mean values of E/E_0 is calculated in each box (both limited by for example the total cloudiness and sun height). These tests have not provide any better results then the tests described earlier and are therefore not described in this report.

4.3 Results

From the tests in the previous chapter, the CMM in test number 3, where mean values of E/E_0 is applied together with a small adjustment to correct the cloud effect for overcast sky, will be used to model all UV for the period 1980-2000. This chapter will illustrate the CMMs performance for different sky conditions, seasons and between the stations listed in Table 3.2. Also all integration periods, hourly, monthly and yearly, will be considered.

For validation of hourly UV, still only independent observations are used. But to calculate daily, monthly and yearly values from the independent validation observations is impossible. The independent hourly observations have been separated with a chance generator from the data used in the estimation of the CMMs, days are separated, and also some months are missing, because of the low sun height. Therefore, all available observations listed in Table 3.2 are used in the validation of daily, monthly and yearly values.

As shown in Chapter 4.2 the modelled hourly UV is on average 3.4% higher than the observed UV. To investigate this, a look at both the frequency of observed and modelled data in different UV intervals has been studied and also the model characteristics for different amounts of cloud. The frequency distribution of both observed and modelled UV in 7 UV intervals is illustrated in Figure 4.12. In all UV intervals except in the lowest (UV<20 mWh/m²) and the highest (UV>120 mWh/m²) intervals the modelled data has a higher frequency than the observed data. The discrepancy in the lowest interval does not necessary only depend on an overestimation of UV in the model, it might also be partly caused by systematic errors of the observed values for low solar altitudes. The UV intervals in Figure 4.12 can be interpreted as different seasons, the lowest UV intervals is strongly influenced by winter and spring/autumn values and the highest intervals by summer values but also as different amounts of clouds.

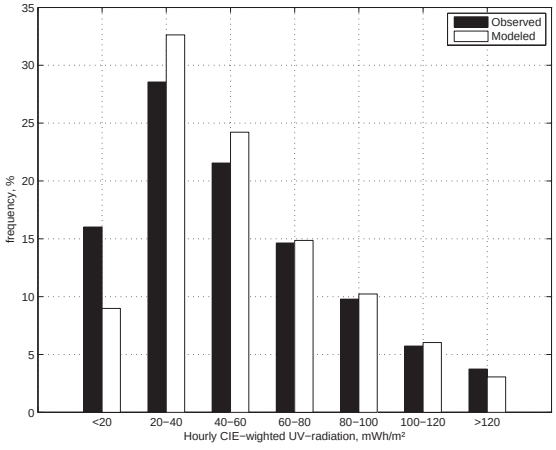

Figure 4.12: Frequency distributions of hourly UV in percentage of the total amounts of samples separated in 7 UV intervals. The black bars correspond to the amount of observed UV in each interval as the percentage of the total amount of observed UV. The white bars instead correspond to the amount of modelled UV in each interval as the percentage of the total amount of modelled UV.

How the modelled UV in relation to the observed UV for different cloud amounts behaves is illustrated in Figure 4.13 as scatter plots for modelled versus observed UV for different cloud amounts. The scatter plots show that for small amounts of cloud (cloudiness less the 4/8 in Figure 4.13) the UV is very much correlated to the modelled data, except for the cases when the observations is affected by clouds and the modelled data is not (the black dots above the 1:1 line). In these cases the modelled UV is overestimated. For the other cases, when the cloudiness is greater then 4/8 also the feature when the modelled data has more cloudiness then the observation is getting more mark able (the black dots below the 1:1 line). It is only when the sky is almost overcast and overcast (5-8/8 cloudiness) the modelled UV data is in average underestimated, otherwise the samples when the observed data has clouds and the modelled data has less cloudiness is in majority.

One reason for the discrepancy between modelled and measured data for various cloud amounts is that the cloudiness is generated in the model area and not analysed. Therefore, the dynamics of the model may create clouds with a slight shift in space and time. Although, the cloud climate is in general correct while the individual hourly values may differ from the observed. Most of the features of Figure 4.13 can be understood from this point of view.

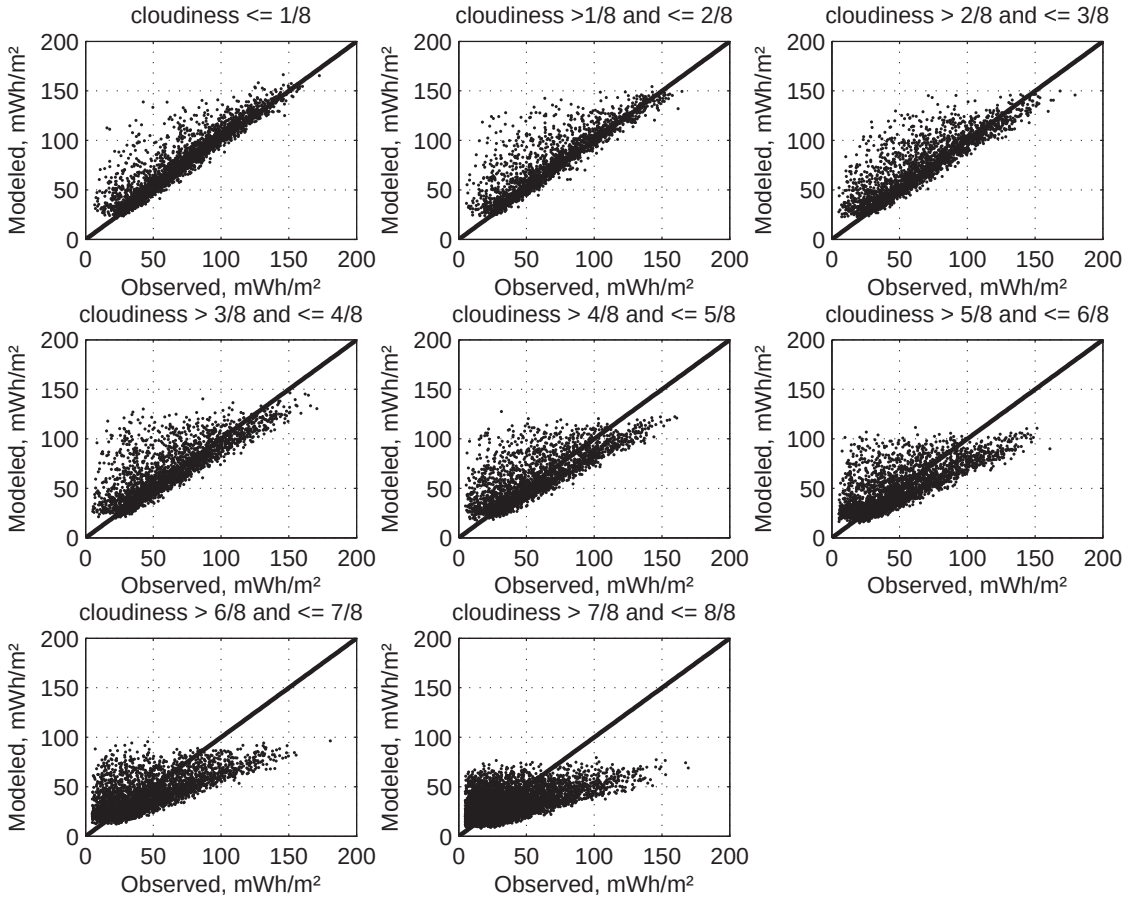

Figure 4.13: Scatter plots for hourly UV, modelled versus observed. The panels illustrate different amounts of total cloudiness from the model, from clear sky (top left) to overcast sky (bottom, middle).

Now the performance of the model depending on the amount of UV and amount of cloudiness have been studied, it is then necessary to investigate if the hourly UV errors might be dependent of the observation location. That is, if the observation point is representative for the whole grid box or not? To investigate this, error calculations have been done for each station separately. It is here important to remember that the amount of samples for each station is very varying since only the samples with sun height above or equal to 25° have been used, then many samples disappears for the most northern stations. The errors for each station are plotted in Figure 4.14. On the x-axes are the stations from south to north (Landvik, Norrköping, Blindern, Østerås, Kise, Trondheim and Tromsö). As seen in Figure 4.14, the RMSD is very much the same for all stations, but the largest one is found in Tromsö. Also the most pronounced MBD is found in Tromsö. Otherwise the modelled UV is very much the same, the MBD is the error quantity shifting most, from an overestimation of 9% in Landvik to an underestimation of 12% for Tromsö, for the other station the MBD is much less pronounced. Landvik and Tromsö are the most problematical stations of the validation stations. Landvik is a coast station and so is Tromsö, together with a location at very high latitude, and the town is also placed inside a valley.

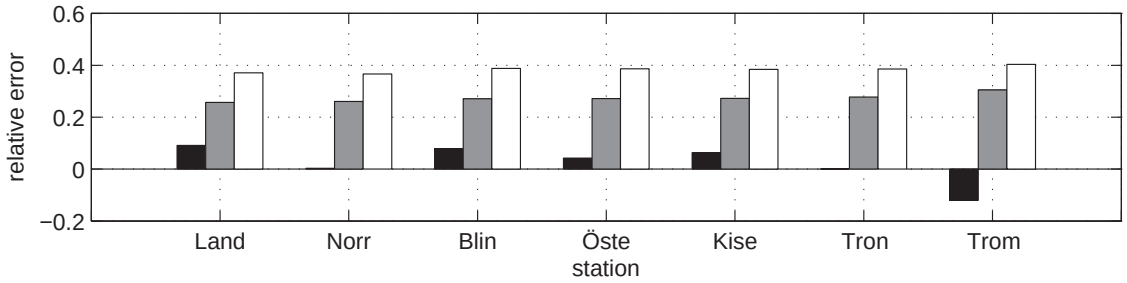

Figure 4.14: MBD (black bars), MAD (grey bars) and RMSD (white bars) calculated for hourly UV for each station separately. From the most southern (Landvik) to the most northern station (Tromsö) listed in Table 3.2.

The hourly relative errors separated to each month have also been studied and are illustrated in Figure 4.15. January, February, November and December are missing in the graph since the sun height for those months is not above or equal to 25°. The hourly errors are very much the same for all the studied months.

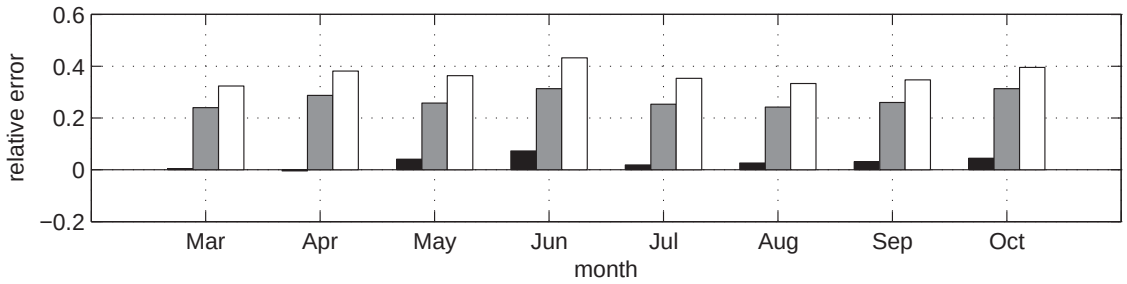

Figure 4.15: The hourly relative errors, MBD (black bars), MAD (grey bars) and RMSD (white bars) have here been calculated for each month separately.

Finally a look at daily, monthly and yearly UV values will be done. As mentioned earlier it is not possible to calculate daily, monthly and yearly values using the

independent observations. Therefore all available observations listed in Table 3.2 are used in the validation of daily, monthly and yearly value. In Table 4.4 the daily, monthly and yearly errors (MBD, MAD and RMSD) are listed.

Table 4.4: List of MBD, MAD and RMSD for daily, monthly and yearly values of UV, calculated for all available observations listed in Table 3.2.

	Daily	**Monthly**	**Yearly**
MBD	+2.6%	+2.6%	+2.6%
MAD	22.0%	8.3%	6.1%
RMSD	38.0%	13.8%	7.6%

Here, a slightly overestimation exists, the other errors (MAD and RMSD) decreases with the length of the integration period. In Figure 4.16 the corresponding scatter plots for daily, monthly and yearly values are plotted, also the hourly scatter plot for all available data, without any limitation in the sun height is plotted in the same figure.

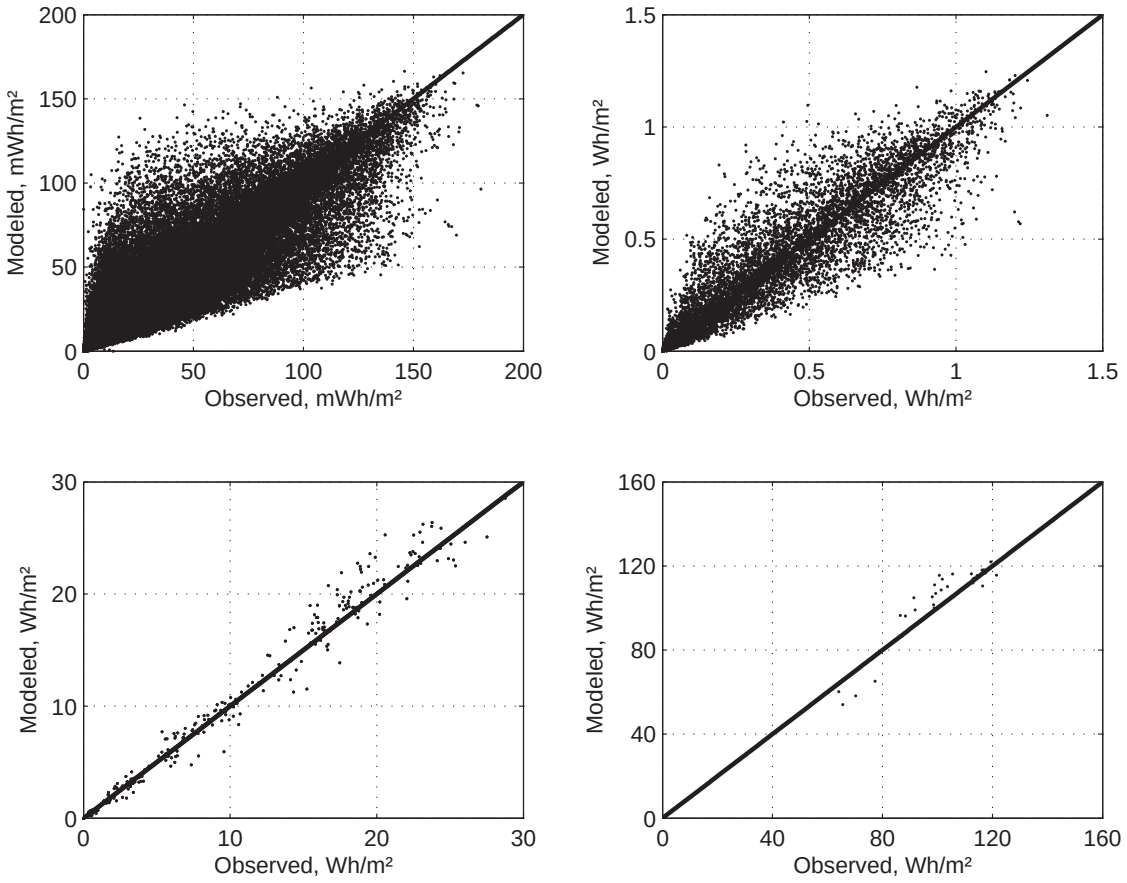

Figure 4.16: Scatter plots for modelled UV versus observed UV for hourly values (top left), daily values (top right), monthly values (bottom left) and for yearly values (bottom right).

Also the daily and monthly errors for each station separately have been calculated, as for the hourly values (Figure 4.14) and are illustrated as histograms in Figure 4.17. The yearly errors are not calculated since many of the stations only has some few years of measurements, then the error might not be representative. The largest errors are found in

Tromsö, as for the hourly values (see Figure 4.14), probably because of the problematic topography and vicinity to the sea. Otherwise a small underestimation is found in Norrköping and Tromsö (negative MBD) and for the other station a small overestimation is found (positive MBD). Yearly UV values for each station can instead be found as time series in the Appendix, Figure 2. Missing in the figure are the stations Trondheim and Østerås since only observations for 1999-2000 are available. The time series can not be used for trend studies since only available measured observations not interpolated observations have been used.

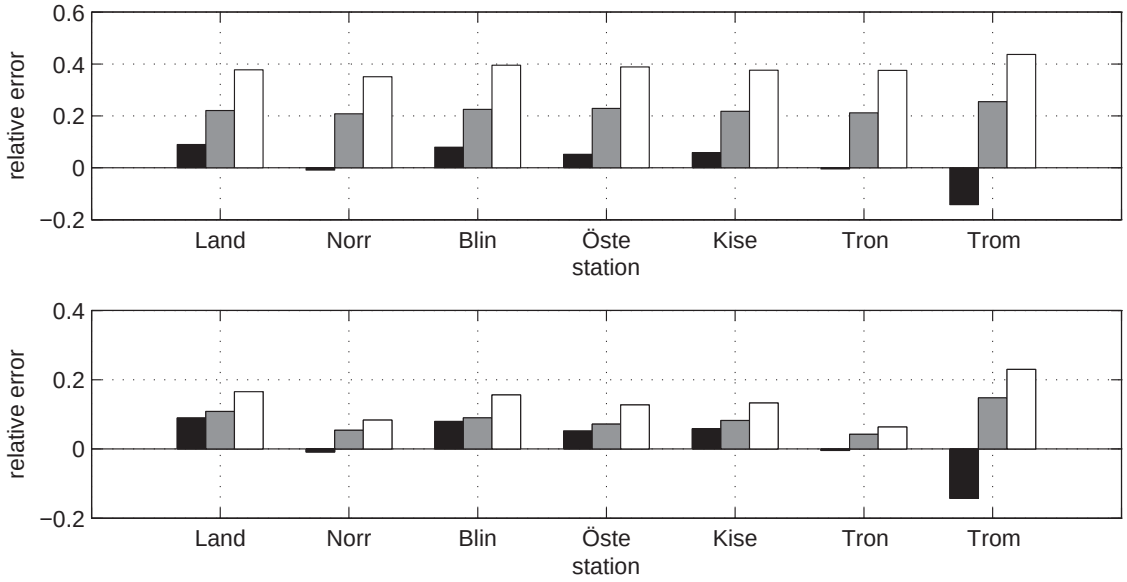

Figure 4.17: Histograms for MBD (black bars), MAD (grey bars) and RMSD (white bars) between modelled and observed UV for each station individual, from south (Landvik) to north (Tromsö). Top: For daily values. Middle: for monthly values. Bottom: for yearly values. Note that the y-axis is shifting.

5 Global radiation

The global radiation originates from the RCA3 model and has been validated for clear sky and cloudiness sky. Attention to hourly, daily, monthly and yearly values has been done. For calculation of the hourly errors only values when the sun height is above or equal to 25º have been used, otherwise the relative error for small amounts of global radiation will take over.

5.1 Clear sky

The clear sky global radiation from the RCA3 model has here been validated against the observations listed in Table 3.3. The clear sky is here defined as when the observed sunshine duration is one hour per hour and the total cloudiness from the RCA3 model is less then 3%, this gives totally 13575 samples. In the left panel in Figure 5.1 the clear sky global radiation, when both the observations and the model has clear sky is plotted as modelled versus observed global radiation. In the graph it is seen that the modelled data is a bit to low compared to the observations for high amounts of global radiation (the black dots below the 1:1 line in Figure 5.1, left). But for low amounts of global

radiation the opposite occurs, the modelled global radiation is instead higher then the observations (the black dots above the 1:1 line in Figure 5.1, left). Therefore it is possible that the biases are dependent on the sun height, and a test also indicates that this is the case. So a correction for the global radiation dependent on the sun height has been created. This correction has not only been done for the clear sky global radiation, but for all sky conditions. The corrections have been calculated as the median values of the quota between observed and modelled global radiation in 21 intervals of the sun height (25-60°).

The corrected modelled clear sky versus observed global radiation is plotted in Figure 5.1, right). Here it is evident that the samples are much closer to the 1:1 line. In the new corrected modelled global radiation the bias is -0.8%, the MAD is 3.4% and the RMSD is 4.5%. Before the correction on the global radiation were made the deviations were instead, MBD = -2.8%, MAD = 4.2% and RMSD = 5.1%.

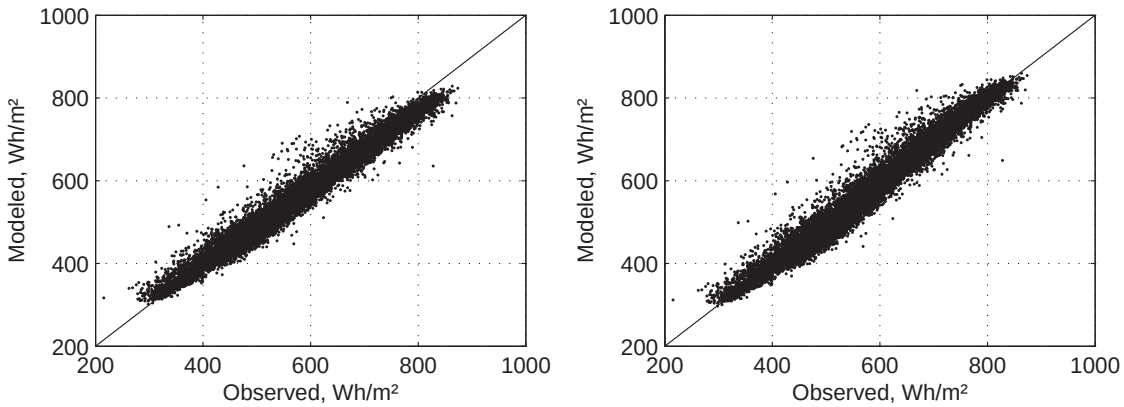

Figure 5.1: Scatter plots for hourly clear sky global radiation when the sun height is above or equal to 25°. The data originates from all 12 radiation stations in Sweden, modelled versus observations for the years 1983-2000. The panel to the left corresponds to the original clear sky global radiation and the panel to the right, the corrected clear sky global radiation. The black line in both panels corresponds to the 1:1 line.

If the clear sky errors instead are calculated when only the observations indicates clear sky (sunshine duration is one hour per hour), independent of the modelled cloudiness, the errors will increase. This will happen because there are cases when the observations have clear sky and the model has cloudy sky. In this case the clear sky statistics are instead, MBD = -13.5%, MAD = 5.6% and RMSD = 24.1%. There are mainly two factors that may explain these deviations. First, we compare values measured at a point with values modelled for an area. Second, sunshine duration can be recorded even when the sky is partly covered by relatively thick clouds, for example with cumulus clouds during summertime. So the sky may not be as clear as indicated by the sunshine duration observation. Also the fact that the model does not include any data assimilation, i.e., cloud system might come earlier or later than in the real world has a large impact to this error.

5.2 All sky conditions

For all cases, i.e. independent of the sunshine duration from the observations and the cloudiness from RCA3, the data constitutes of 1835236 samples and for the cases when the sun height is above or equal to 25º it constitutes of 342189 samples.

As described earlier, a correction dependent on the sun height have been applied on all modelled data, independent of the sky condition. Before the correction is made, the biases more or less balance each other, i.e. the underestimation of high global radiation values is compensated by the overestimation of low global radiation values (this can even be seen for the clear sky, Figure 5.1). The correction made removes the underestimation of high global radiation amounts, and a part of the overestimation of low values. But we does make sure that the most important situations for this project will be as correct as possible, clear sky in combination with high sun altitude. The reason why the overestimation of low values not are reduced sufficient depends probably on all samples in the data set when the model has clear sky and the observations has cloudy sky. We can not separately extract these cases of the model, only the cases when the model already has clouds, but they are to thin.

For all samples, i.e., for all sky conditions, the MBD, MAD and RMSD have been calculated for hourly (when the sun height is above or equal to 25º), daily, monthly and yearly values. The statistics is listed in Table 5.1. For the MBD, a positive sign indicates that the modelled data are higher then the observed values. All daily, monthly and yearly values have been calculated independent on the amounts of available observations for each time period, i.e. yearly values have been calculate even if only one month is available, therefore some very small yearly values exists, also, it influence the error in a negative matter, i.e. the yearly error corresponds to much shorter periods and in that way also the errors.

Table 5.1: MBD, MAD and RMSD for hourly, daily, monthly and yearly values for global radiation between RCA3 and observations for the years 1983-2000.

	Hourly	**Daily**	**Monthly**	**Yearly**
MBD	+1.7%	+1.6%	+1.6%	+1.6%
MAD	32.2%	25.4%	9.8%	4.4%
RMSD	43.5%	41.1%	14.3%	5.4%

The MBD indicates that there is a small overestimation of the global radiation. This is mainly caused by the underestimation of clouds in the model, which we could not correct for. The hourly errors is relatively large which of course depends on the difficulties in making cloud analysis without any data assimilation in the model, the model only force information in to the model domain through the lateral boundaries. It is then very easy to get for example a cold front together with its clouds to get behind the real world. But for longer time periods this feature decreases with the length of the time period. Figure 5.2 shows the scatter plots for daily (top left), monthly (top right) and yearly (bottom left) values.

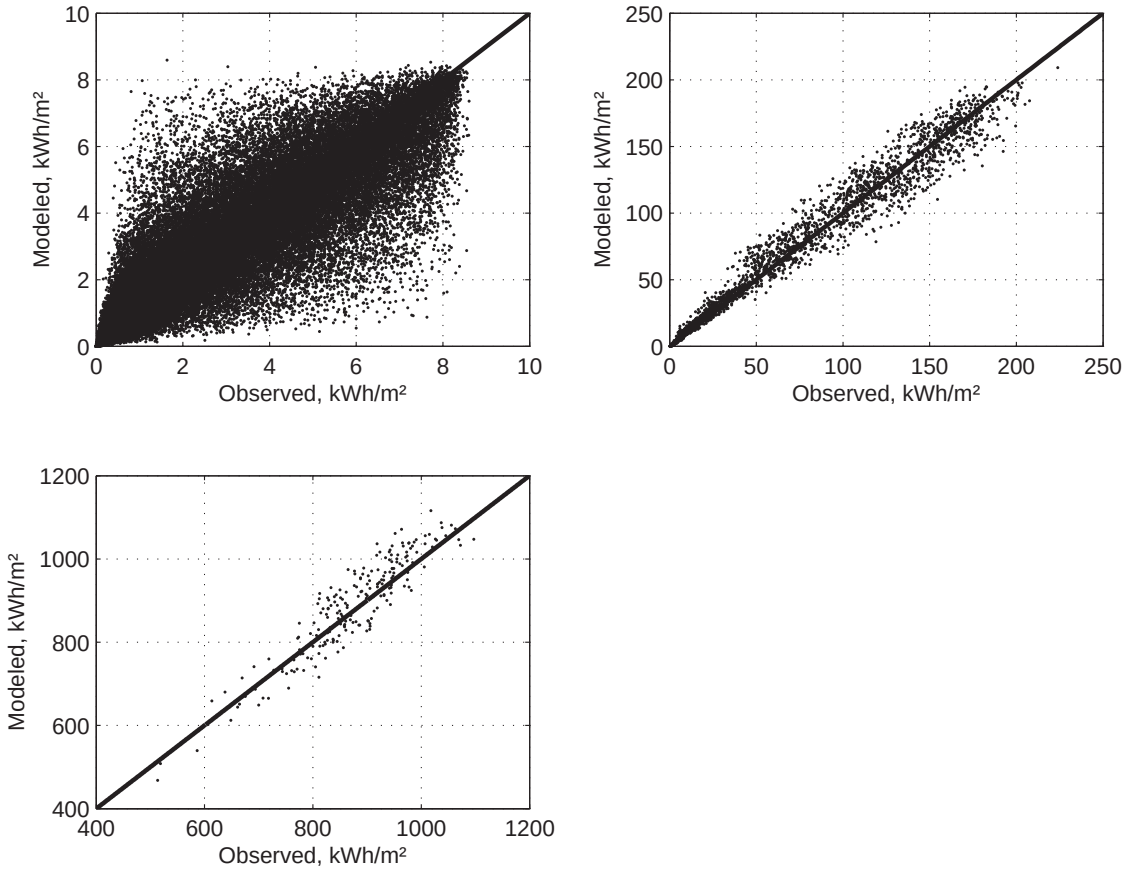

Figure 5.2: Scatter plots for global radiation for all available observations during 1983-2000. Top left: for daily values, Top right: for monthly values, bottom left: for yearly values.

To show the behaviour of the model for different geographical sites, the errors for each station individual has been calculated. The radiation stations in Sweden cover almost the whole country, from south to north, and it will be a good indicator how the model for example represent the snow cover. The daily (top panel) and monthly (bottom panel) relative errors (MBD, MAD and RMSD) for each station are illustrated as histograms in Figure 5.3. The x-axis corresponds to the stations from north (Kiruna) to south (Lund). The MAD and RMSD are very similar for all stations. The MBD is on the other hand a bit shifting from station to station. For both daily and monthly values, almost all northern stations have a systematic lower modelled global radiation compared to the observations. The more southern stations have instead a systematic higher modelled global radiation compared to the observed values. As mentioned earlier the underestimation of global radiation for the more northern station could be caused by the difficulties in representing the snow cover in the albedo. But even if the snow cover is well represented in the model it might still be problems since the albedo in the model represents an area and the observations are made at a point.

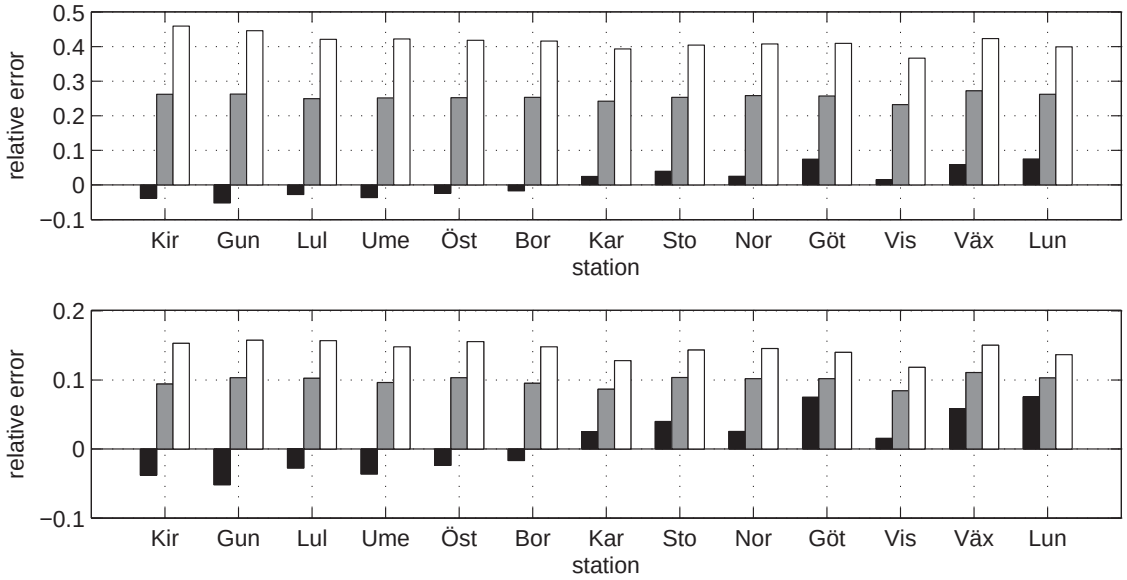

Figure 5.3: The daily (top) and monthly (bottom) MBD (black bars), MAD (grey bars) and RMSD (white bars) have been calculated for each radiation station in Sweden individually for 1983-2000. From left to right are the stations from north to south. Note that the y-axes not are the same.

For seasonal discrepancies, the daily errors have been calculated for each month separately, see Figure 5.4. As for the daily and monthly biases calculated for each station (Figure 5.3) the snow seems to have influence on the biases for the winter months. Also during the winter months the largest RMSD and MAD occur, this features depends not only on the difficulties in representing a good snow cover, it also depends on the small amounts of global radiation during wintertime, which makes the relatively errors large. Otherwise the errors during the summer months are the smallest ones. The modelled data has a systematic higher amount of radiation during the summer months (June-September) and the opposite during the winter months.

Examples on yearly time series are illustrated in Figure 3, 4 and 5 in the Appendix. The graphs show the observed and modelled yearly amounts of global radiation for all radiation stations in Sweden (Table 3.3), except Gunnarn, since only 4 years are available. The time series can not be used for studying trends, since only available measurements have been used, not any interpolated values replacing missing values. The positive bias for the modelled global radiation on average (Table 5.1) is most pronounced for the southern stations (Figure 4, Appendix) while the bias is minimal for the more northern stations (Figure 3, Appendix). The same feature is also seen in the daily and monthly values i.e., positive bias for southern station and a slight underestimation for northern stations (Figure 5.2 and 5.3)

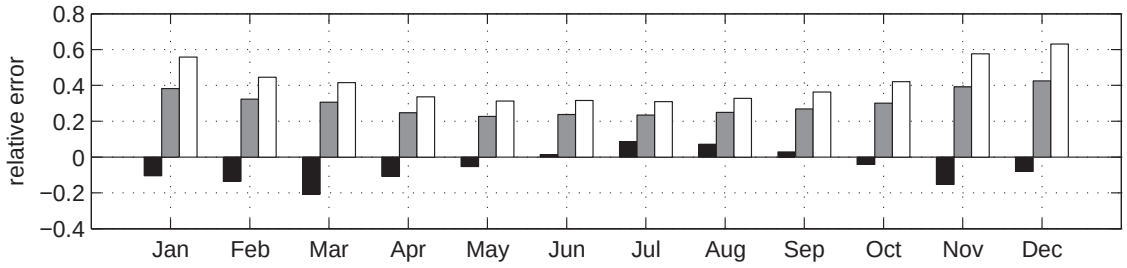

Figure 5.4: The daily relative errors, MBD, MAD and RMSD have here been calculated for each month separately.

6 Available output data

All fields of CIE-weighted UV-radiation and global radiation created in this project on hourly, daily, monthly and yearly basis for the period 1980-2000 are all stored in GRIB-format (GrIdded Binary). The spatial resolution is 22x22 km with a rotated latitude-longitude coordinate system. The fields are stored in 102 grid points in west-east direction and 116 grid points in south-north direction, i.e. a total of 11832 grid points. All data can be studied and retrieved at the web interface, www.smhi.se/strang/omna. There are three options at the interface. All options are valid for both global radiation and CIE-weighted UV-radiation for the whole period (1980-2000) and for hourly, daily, monthly and yearly values. The options are:

1) To select charts.
2) To retrieve time series for an optional point, given in latitude and longitude.
3) To retrieve fields.

It is important to remember that all hours at the web interface are given in UTC and not local time. Also, the daily, monthly and yearly values are summarized hourly values. In Figure 6.1 an example from the web-interface is given, here monthly charts for global radiation and CIE-weighted UV-radiation for April 1998 has been chosen. The white area at the west, south and east side in Figure 6.1 is the new extended model domain for the STRÅNG-system (www.smhi.se/strang).

Another example that can be selected from the web interface is yearly time series for CIE-weighted UV-radiation and global radiation. In Figure 6.2 such time series is plotted for four sites in Sweden, namely Luleå, Karlstad, Stockholm and Lund.

Also delivered with this project are integrated daily county values for global radiation and CIE-weighted UV-radiation. The county areas are selected from the red map (SW. röda kartan) and cut of over the sea areas by the Swedish territorial border. A map together with the Swedish territorial border is presented in the Appendix, Figure 1, also a list of the county names can be found in the Appendix, Table 1.

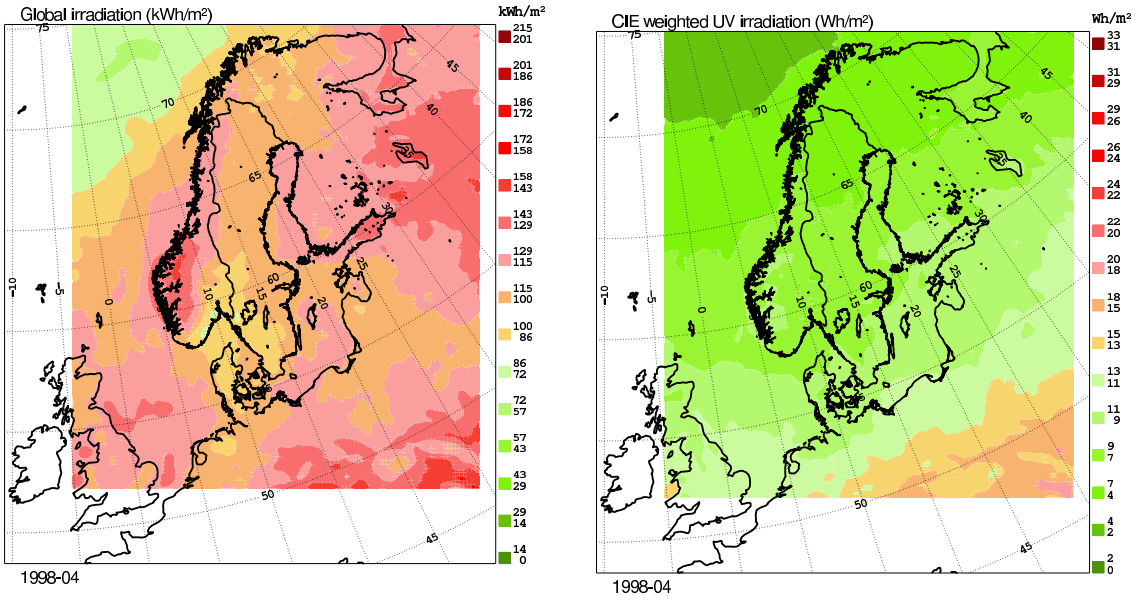

Figure 6.1: Monthly global radiation (left) and CIE-weighted UV-radiation (right) selected from the web interface for April 1998.

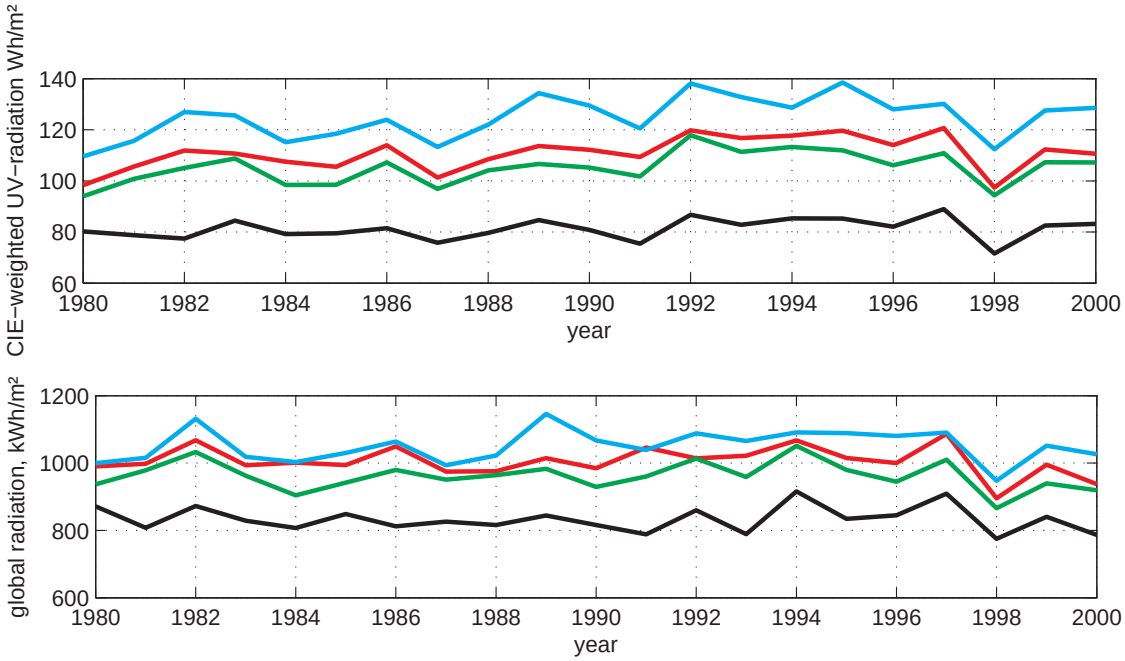

Figure 6.2: Yearly time series for modelled CIE-weighted UV-radiation (top), and global radiation (bottom) for Luleå (black line), Karlstad (red line), Stockholm (green line) and Lund (blue line).

7 Discussion and Conclusions

A data set with CIE-weighted UV-radiation and global radiation on hourly basis for the period 1980-2000 over northwest Europe has been created in this project. The approach to create the data set has been to use consistent data both in time and space. In that way the origin of trends in the data set is reduced to not depend on changes in the atmospheric models.

Since the data set shall cover a relatively long period (1980-2000), no high resolution gridded meteorological analyses exist at SMHI for the whole period. For shorter time periods (1998-today) a high resolution mesoscale model called MESAN is often used. The model combines information from a Numerical Weather Prediction forecast, radar, satellites and ground based observations to a 2-dimensional field covering northwest Europe with a fine spatial (11x11 km) and temporal resolution (1 hour). But because of the long time period that is needed in this project this data could not be used, instead the data has to originate from other sources.

One choice of input data sources in this project has been the ERA-40 data set which is a comprehensive set of time consistent data describing the state of the atmosphere for the whole globe. From the ERA-40 data set the total column ozone analysis has been used once a day. The ERA-40 ozone has been corrected for systematic errors and errors due to missing satellite data in the ERA-40 data assimilation routine. Validation of the corrected ERA-40 against observations shows that the ozone is very well represented in the ERA-40 analysis. For the other needed parameters in this project, global radiation and cloud information, it is not possible to use the ERA-40 data set since the temporal resolution is limited to every six hour. Otherwise it would probably be one of the best choice of input data since a large set of different kinds of observations (satellites, ground based observations and so on) are assimilated in the analysis and that the data are produced with one and the same method for the whole time period (September 1959 to August 2002). The global radiation and cloud information have instead been selected from the new version of the Rossby Regional Climate Atmospheric model (RCA3). The RCA3 model is not a model that assimilates different kinds of observations in to the model. Instead, it forces a global re-analysis, in this case the ERA-40, in to the model through the lateral boundaries. In that way a much finer spatial and temporal resolution can be achieved over a limited area. The model is based on the operational regional weather prediction model HIRLAM but with process formulations and parameterizations adjusted to suit long-term climate simulations.

Beside of all modelled data a relatively large set of UV-measurements has been used to create the CIE-weighted UV-radiation data set in this project.

Since the future use of this data set is focused on skin cancer statistics, the main aim has been to keep the errors small when the risk of development skin cancer are most pronounced, i.e., when the sun is high and the sky is relatively clear. This holds for both CIE-weighted UV-radiation and global radiation.

For CIE-weighted UV-radiation the model is divided in to two modules, in the first one, the clear sky CIE-weighted UV-radiation is modelled for each hour. In this module, a “lookup table” was first produced with the FastRT model. In the “lookup table” all variations of input parameters are taken into account. In a multi-dimensional spline interpolation the clear sky UV for all years are modelled. The main input parameters to

the “lookup table” are the Ångström turbidity coefficient, the solar zenith angle, the total ozone column, and the albedo.

In the second module, the clear sky modelled CIE-weighted UV-radiation, created in module one, is reduced using a cloud modification model (CMM). The construction of the cloud modification model has been tested in several ways. In all tests a set of independent observations have been used in the estimation of the CMMs and another set of independent observations have been used in the validation of the outputs from the different CMMs.

Since a large scatter exists in hourly CIE-weighted UV-radiation comparing the observations versus the modelled values it is difficult to find a good CMM (for instance when the model has clear sky and the real word has cloudy sky). As mentioned earlier, our goal has been that the modelled values shall be as good as possible when the sun is high and the sky is relatively clear. The CMM that have been used is a predefined formula that has been fitted to the data. For clear sky the formula does not reduce the clear sky UV, but for overcast skies, the CMM shows that an overestimation of UV still exists in the model. This, because these samples are difficult to model.

The bias for the hourly CIE-weighted UV-radiation is then 3.4% and the root mean square deviation is about 38%, when the sun height is above or equal to 25°. For daily, monthly and yearly amounts of CIE-weighted UV-radiation the modelled values are 2.6% higher than the observations. The root mean square deviation is reduced the longer the integration period is; to 7% for yearly values.

The global radiation from the RCA3 model underestimates the high values and overestimates the low values of global radiation. To overcome this problem a correction factor dependent on the sun height has been applied on the global radiation. In this way the clear sky global radiation is corrected, but low amounts still are slightly overestimated. One reason could be that the model underestimates the cloudiness or that the modelled clouds are to thin. The errors, both for hourly, daily, monthly and yearly values are of the same magnitude as for the CIE-weighted UV-radiation.

As described for both CIE-weighted UV-radiation and global radiation the hourly errors are relatively large but the errors are reduced the longer the time periods are. The main reason for the large hourly errors are that the input data that plays a big role to the CIE-weighted UV-radiation and global radiation fields originates from a downscaling model and not a data assimilation model. Today we do not have access to any data base with high resolution both in time and space fur such a long time period that are needed in this project.

The RCA3 model is often used in climate scenarios projects in Europe and is known to analyse the climate well. Therefore we assume that the created data set should not include any trends caused by the model.

The whole data set is freely available for non-commercial use and can be downloaded at the web-interface, www.smhi.se/strang/omna. Here both time series for eligible points, charts and fields can be chosen for both, hourly, daily, monthly and yearly values of CIE-weighted UV-radiation and global radiation for the period 1980-2000.

Acknowledgments

First we acknowledge the funding from the Swedish Radiation Protection Authority (SSI) on behalf of “Miljömålsrådet”. We also thank Tomas Landelius, SMHI for his valuable advices and recommendations during the whole project. Also to Ulrika Willén and Anders Ullerstig at the Rossby Centre at SMHI who have provided us with RCA3 analyses and helped us interpret the results. We are also grateful to Bjørn Johnsen and his colleagues at NRPA for the supply of Norwegian data as well as to all hard work that lies behind the observations of total ozone and solar radiation by our colleagues in many countries.

References

Carlund, T., Landelius, T., and Josefsson, W. (2003). Comparison and uncertainty of aerosol optical depth estimates derived from spectral and broadband measurements. *J. Appl. Meteorol., 42:11*, 1598-1610.

Engelsen, O. and Kylling, A. (2005). Fast simulation tool for ultraviolet radiation at the Earth's surface. *Optical Engineering*, 44 (4).

Häggmark, L., Ivarsson, K-I., Gollvik, S. and Olofsson, P-O. (2000). Mesan, an operational meso-scale analysis system. *Tellus*, 52, A:2-20.

Kasten, F. and Czeplak, G. (1980). Solar and terrestrial radiation dependence on the amount and type of cloud. *Solar Energy*, 43(34):177-190.

Kjällström, E., Bärring, L., Gollvik, S., Hansson, U., Jones, C., Samuelsson, P., Rummukainen, M., Ullerstig, A., Willén, U. and Wyser, K. (2005). A 140-year simulation of European climate with the new version of the Rossby Centre regional atmospheric climate model (RCA3). SMHI Reports Meteorology and Climatology No. 108, SE-60176 Norrköping, Sweden, 54 pp.

Landelius, T., Josefsson, W. and Persson, T. (2001). A system for modelling solar radiation parameters with mesoscale spatial resolution. SMHI Reports Meteorology and Climatology No 96, SE-60176 Norrköping, Sweden, 52 pp.

McKinley, A.F. and Diffey, B.L. (1987). A reference spectrum for ultraviolet induced erythema in human skin, *CIE-Journal 6*: 17-22.

Rummukainen, M., Räisänen, J., Ullerstig, A., Bringfelt, B., Hansson, U., Graham, P. and Willén, U. (1998). RCA - Rossby Centre regional Atmospheric climate model: model description and results from the first muti-year simulation. SMHI Reports Meteorology and Climatology No. 83, SE-60176 Norrköping, Sweden, 76 pp.

Undén, P., Rontu, L., Järvinen H., Lynch, P., Calvo, J., Cats, G., Cuxart, J., Eerola, K., Fortelius, C., Garcia-Moya, J. A., Jones, C., Lenderlink, G., McDonald, A., McGrath, R., Navascues, B., Nielsen, N. W., Ødegaard, V., Rodriguez, E., Rummukainen, M., Rõõm, R., Sattler, K., Hansen Sass, B., Savijärvi, H., Wichers Schreur, B., Sigg, R., The, H. and Tijm, A. (2002). HIRLAM-5 Scientific Documentation. Available at SMHI, S-60176 Norrköping

Uppala, S. M., Kållberg, P. W., Simmons, A. J., Andrae, U., Da Costa Bechtold, V., Fiorino, M., Gibson, J. K., Haseler, J., Hernandez, A, Kelly, G. A., Li, X., Onogi, K., Saarinen, S., Sokka, N., Allan, R. P., Andersson, E., Arpe, K., Balmaseda, M. A., Beljaars, A. C. M., Van De Berg, L., Bidlot, J., Bormann, N., Caires, S., Chevallier, F., Dethof, A., Dragosavac, M., Fisher, M., Fuentes, M., Hagemann, S., Hólm, E., Hoskins, B. J., Isaksen, L., Janssen, P. A. E. M., Jenne, R., Mcnally, A. P., Mahfouf, J.-F., Morcrette, J.-J., Rayner, N. A., Saunders, R. W., Simon, P., Sterl, A., Trenberth, K. E., Untch, A., Vasiljevic, D., Viterbo, P. and Woollen, J. (2005). The ERA-40 re-analysis. *Q.J.R. Meteorol. Soc., 131,* 2961-3012.

Appendix

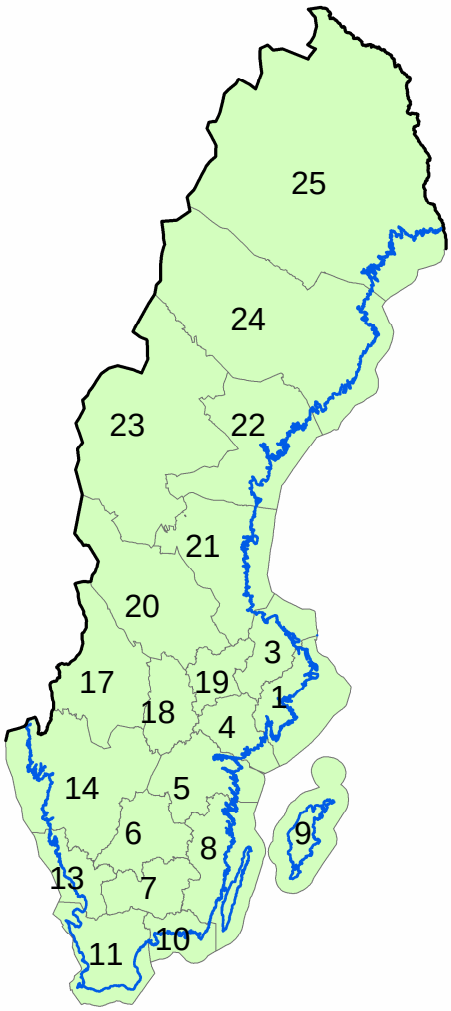

Figure 1: Map over each county from the red map (*röda kartan*).

Table 1: List of all county number and the corresponding name.

Number	**County**
1	Stockholms
3	Uppsala
4	Södermanlands
5	Östergötlands
6	Jönköpings
7	Kronobergs
8	Kalmar
9	Gotlands
10	Blekinge
11	Skåne
13	Hallands
14	Västra Götalands
17	Värmlands
18	Örebro
19	Västmanlands
20	Kopparbergs
21	Gävleborgs
22	Västernorrlands
23	Jämtlands
24	Västerbottens
25	Norrlands

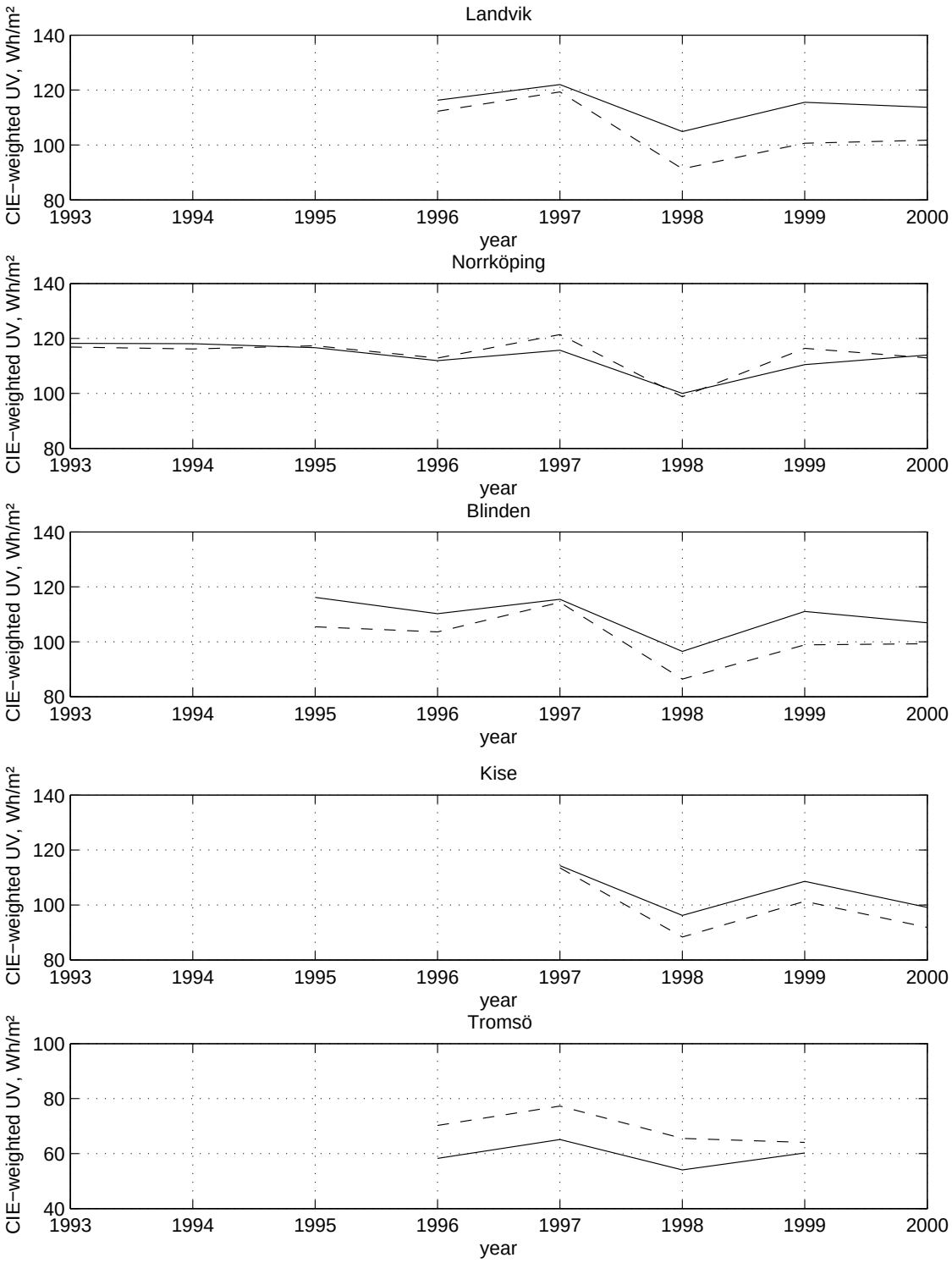

Figure 2: Time series for yearly values of CIE-weighted UV-radiation from the 5 stations with more than 3 years of measurements. The dashed line corresponds in all panels to the observed values and the full line to the modelled values. The time series can not be used for trend studies since months are not always complete as only measured observations are included, no interpolated values have been used for missing values.

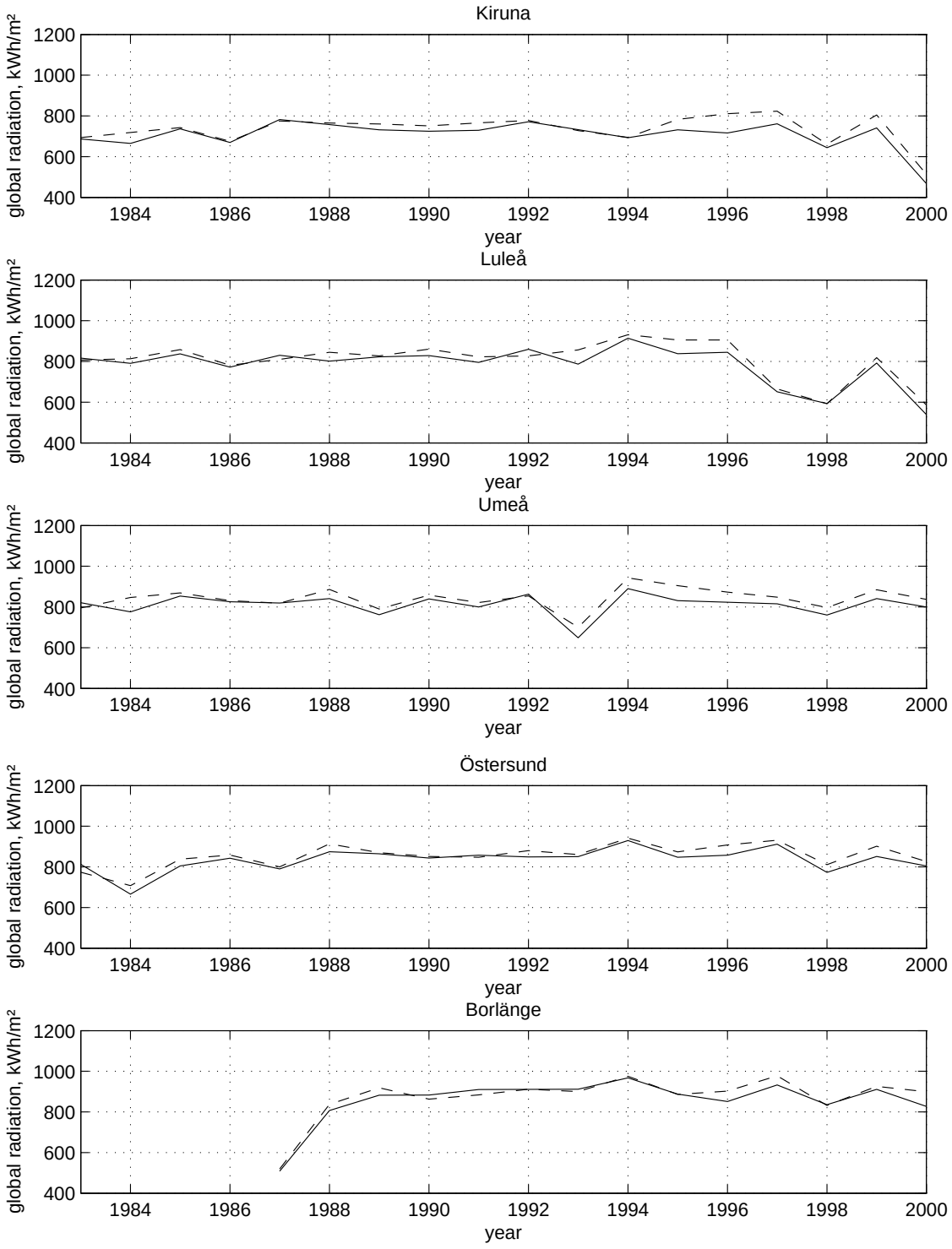

Figure 3: Time series for yearly values of global radiation from the 5 most northern Swedish radiation stations (Kiruna – Borlänge, except Gunnarn since only 4 years of measurements) during 1983-2000. The dashed line corresponds in all panels to the observed values and the full line to the modelled values. The time series can not be used for trend studies since months are not always complete as only measured observations are included, no interpolated values have been used.

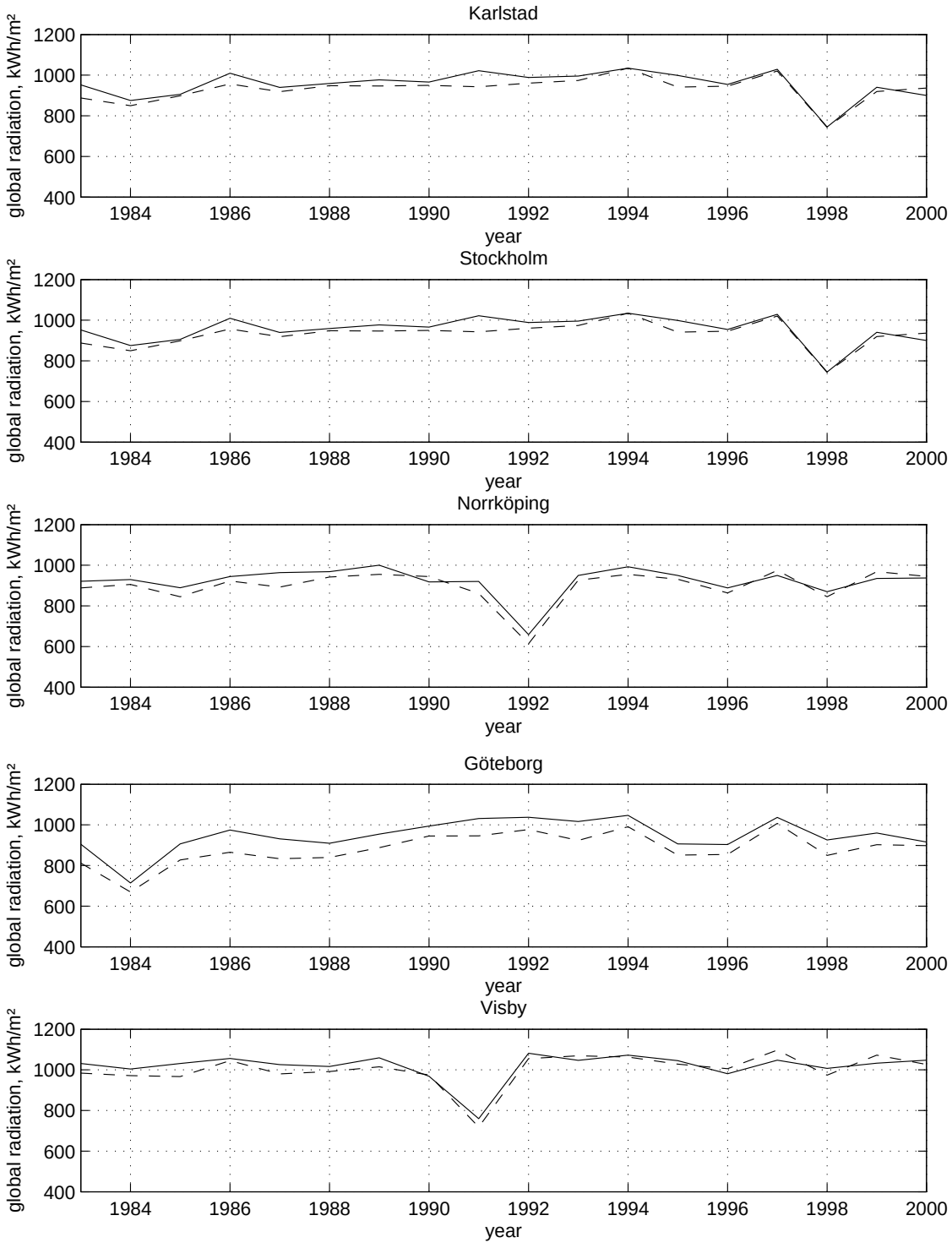

Figure 4: Time series for yearly values of global radiation from Karlstad to Visby during 1983-2000. The dashed line corresponds in all panels to the observed values and the full line to the modelled values. The time series can not be used for trend studies since months are not always complete as only measured observations are included, no interpolated values have been used.

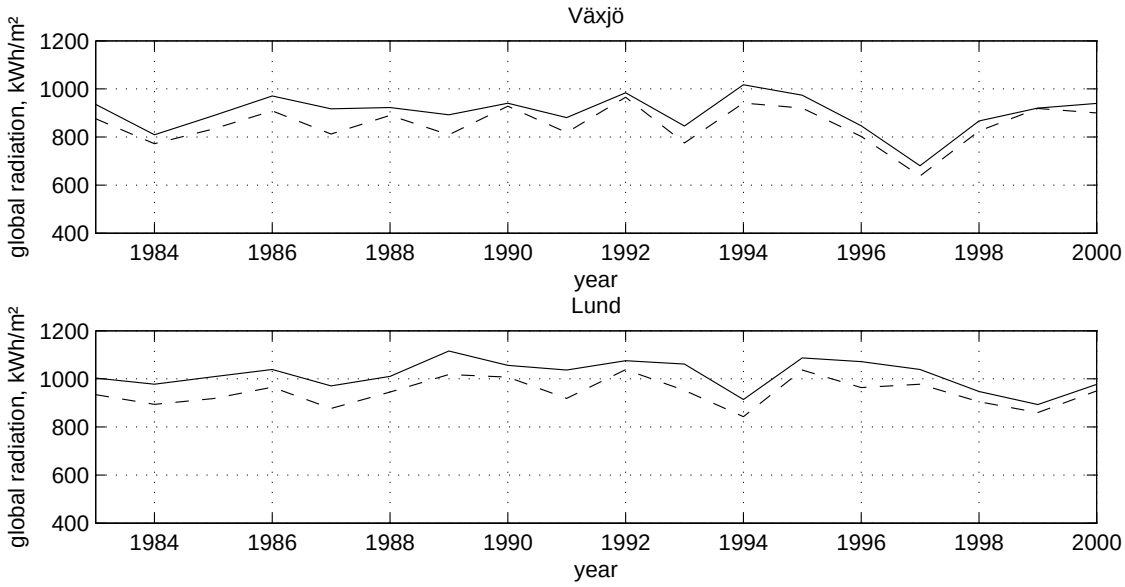

Figure 5: Time series for yearly values of global radiation for the 2 most southern radiation stations in Sweden (Växjö and Lund) during 1983-2000. The dashed line corresponds in all panels to the observed values and the full line to the modelled values. The time series can not be used for trend studies since months are not always complete as only measured observations are included, no interpolated values have been used.

SMHIs publiceringar

SMHI ger ut sex rapportserier. Tre av dessa, R-serierna är avsedda för internationell publik och skrivs därför oftast på engelska. I de övriga serierna används det svenska språket.

Seriernas namn	**Publiceras sedan**
RMK (Rapport Meteorologi och Klimatologi)	1974
RH (Rapport Hydrologi)	1990
RO (Rapport Oceanografi)	1986
METEOROLOGI	1985
HYDROLOGI	1985
OCEANOGRAFI	1985

I serien METEOROLOGI har tidigare utgivits:

1985

1 Hagmarker, A. (1985)
Satellitmeteorologi.

2 Fredriksson, U., Persson, Ch., Laurin, S. (1985)
Helsingborgsluft.

3 Persson, Ch., Wern, L. (1985)
Spridnings- och depositionsberäkningar för av fallsförbränningsanläggningar i Sofielund och Högdalen.

4 Kindell, S. (1985)
Spridningsberäkningar för SUPRAs anläggningar i Köping.

5 Andersson, C., Kvick, T. (1985)
Vindmätningar på tre platser på Gotland. Utvärdering nr 1.

6 Kindell, S. (1985)
Spridningsberäkningar för Ericsson, Ingelstafabriken.

7 Fredriksson, U. (1985)
Spridningsberäkningar för olika plymlyft vid avfallsvärmeverket Sävenäs.

8 Fredriksson, U., Persson, Ch. (1985)
NO_x- och NO_2-beräkningar vid Vasaterminalen i Stockholm.

9 Wern, L. (1985)
Spridningsberäkningar för ASEA transformers i Ludvika.

10 Axelsson, G., Eklind, R. (1985)
Ovädret på Östersjön 23 juli 1985.

11 Laurin, S., Bringfelt, B. (1985)
Spridningsmodell för kväveoxider i gatumiljö.

12 Persson, Ch., Wern, L. (1985)
Spridnings- och depositionsberäkningar för avfallsförbränningsanläggning i Sofielund.

13 Persson, Ch., Wern, L. (1985)
Spridnings- och depositionsberäkningar för avfallsförbränningsanläggning i Högdalen.

14 Vedin, H., Andersson, C. (1985)
Extrema köldperioder i Stockholm.

15 Krieg, R., Omstedt, G. (1985)
Spridningsberäkningar för Volvos planerade bilfabrik i Uddevalla.

16 Kindell, S. Wern, L. (1985)
Luftvårdsstudie avseende industrikombinatet i Nynäshamn (koncentrations- och luktberäkningar).

17 Laurin, S., Persson, Ch. (1985)
Beräknad formaldehydspridning och deposition från SWEDSPANs spånskivefabrik.

18 Persson, Ch., Wern, L. (1985)
Luftvårdsstudie avseende industri-kombinatet i Nynäshamn – depositions-beräkningar av koldamm.

19 Fredriksson, U. (1985)
Luktberäkningar för Bofors Plast i Ljungby, II.

20 Wern, L., Omstedt, G. (1985)
Spridningsberäkningar för Volvos planerade bilfabrik i Uddevalla - energicentralen.

21 Krieg, R., Omstedt, G. (1985)
Spridningsberäkningar för Volvos planerade bilfabrik i Uddevalla - kompletterande beräkningar för fabrikerna.

22 Karlsson, K.-G. (1985)
Information från Meteosat - forskningsrön och operationell tillämpning.

23 Fredriksson, U. (1985)
Spridningsberäkningar för AB Åkerlund & Rausings fabrik i Lund.

24 Färnlöf, S. (1985)
Radarmeteorologi.

25 Ahlström, B., Salomonsson, G. (1985)
Resultat av 5-dygnsprognos till ledning för isbrytarverksamhet vintern 1984-85.

26 Wern, L. (1985)
Avesta stadsmodell.

27 Hultberg, H. (1985)
Statistisk prognos av yttemperatur.

1986

1 Krieg, R., Johansson, L., Andersson, C. (1986)
Vindmätningar i höga master, kvartalsrapport 3/1985.

2 Olsson, L.-E., Kindell, S. (1986)
Air pollution impact assessment for the SABAH timber, pulp and paper complex.

3 Ivarsson, K.-I. (1986)
Resultat av byggväderprognoser - säsongen 1984/85.

4 Persson, Ch., Robertson, L. (1986)
Spridnings- och depositionsberäkningar för en sopförbränningsanläggning i Skövde.

5 Laurin, S. (1986)
Bilavgaser vid intagsplan - Eskilstuna.

6 Robertson, L. (1986)
Koncentrations- och depositionsberäkningar för en sopförbränningsanläggning vid Ryaverken i Borås.

7 Laurin, S. (1986)
Luften i Avesta - föroreningsbidrag från trafiken.

8 Robertson, L., Ring, S. (1986)
Spridningsberäkningar för bromcyan.

9 Wern, L. (1986)
Extrema byvindar i Orrefors.

10 Robertson, L. (1986)
Koncentrations- och depositionsberäkningar för Halmstads avfallsförbränningsanläggning vid Kristinehed.

11 Törnevik, H., Ugnell (1986)
Belastningsprognoser.

12 Joelsson, R. (1986)
Något om användningen av numeriska prognoser på SMHI (i princip rapporten till ECMWF).

13 Krieg, R., Andersson, C. (1986)
Vindmätningar i höga master, kvartalsrapport 4/1985.

14 Dahlgren, L. (1986)
Solmätning vid SMHI.

15 Wern, L. (1986)
Spridningsberäkningar för ett kraftvärmeverk i Sundbyberg.

16 Kindell, S. (1986)
Spridningsberäkningar för Uddevallas fjärrvärmecentral i Hovhult.

17 Häggkvist, K., Persson, Ch., Robertson, L (1986)
Spridningsberäkningar rörande gasutsläpp från ett antal källor inom SSAB Luleåverken.

18 Krieg, R., Wern, L. (1986)
En klimatstudie för Arlanda stad.

19 Vedin, H. (1986)
Extrem arealnederbörd i Sverige.

20 Wern, L. (1986)
Spridningsberäkningar för lösningsmedel i Tibro.

21 Krieg, R., Andersson, C. (1986)
Vindmätningar i höga master - kvartalsrapport 1/1986.

22 Kvick, T. (1986)
Beräkning av vindenergitillgången på några platser i Halland och Bohuslän.

23 Krieg, R., Andersson, C. (1986)
Vindmätningar i höga master - kvartalsrapport 2/1986.

24 Persson, Ch. (SMHI), Rodhe, H. (MISU), De Geer, L.-E. (FOA) (1986)
Tjernobylolyckan - En meteorologisk analys av hur radioaktivitet spreds till Sverige.

25 Fredriksson, U. (1986)
Spridningsberäkningar för Spendrups bryggeri, Grängesberg.

26 Krieg, R. (1986)
Beräkningar av vindenergitillgången på några platser i Skåne.

27 Wern, L., Ring, S. (1986)
Spridningsberäkningar, SSAB.

28 Wern, L., Ring, S. (1986)
Spridningsberäkningar för ny ugn, SSAB II.

29 Wern, L. (1986)
Spridningsberäkningar för Volvo Hallsbergverken.

30 Fredriksson, U. (1986)
SO_2-halter från Hammarbyverket kring ny arena vid Johanneshov.

31 Persson, Ch., Robertson, L., Häggkvist, K. (1986)
Spridningsberäkningar, SSAB - Luleåverken.

32 Kindell, S., Ring, S. (1986)
Spridningsberäkningar för SAABs planerade bilfabrik i Malmö.

33 Wern, L. (1986)
Spridningsberäkningar för svavelsyrafabrik i Falun.

34 Wern, L., Ring, S. (1986)
Spridningsberäkningar för Västhamnsverket HKV1 i Helsingborg.

35 Persson, Ch., Wern, L. (1986)
Beräkningar av svaveldepositionen i Stockholmsområdet.

36 Joelsson, R. (1986)
USAs månadsprognoser.

37 Vakant nr.

38 Krieg, R., Andersson, C. (1986)
Utemiljön vid Kvarnberget, Lysekil.

39 Häggkvist, K. (1986)
Spridningsberäkningar av freon 22 från Ropstens värmepumpverk.

40 Fredriksson, U. (1986)
Vindklassificering av en plats på Hemsön.

41 Nilsson, S. (1986)
Utvärdering av sommarens (1986) använda konvektionsprognoshjälpmedel.

42 Krieg, R., Kvick, T. (1986)
Vindmätningar i höga master.

43 Krieg, R., Fredriksson, U. (1986)
Vindarna över Sverige.

44 Robertson, L. (1986)
Spridningsberäkningar rörande gasutsläpp vid ScanDust i Landskrona - bestämning av cyanvätehalter.

45 Kvick, T., Krieg, R., Robertson, L. (1986)
Vindförhållandena i Sveriges kust- och havsband, rapport nr 2.

46 Fredriksson, U. (1986)
Spridningsberäkningar för en planerad panncentral vid Lindsdal utanför Kalmar.

47 Fredriksson, U. (1986)
Spridningsberäkningar för Volvo BMs fabrik i Landskrona.

48 Fredriksson, U. (1986)
Spridningsberäkningar för ELMO-CALFs fabrik i Svenljunga.

49 Häggkvist, K. (1986)
Spridningsberäkningar rörande gasutsläpp från syrgas- och bensenupplag inom SSAB Luleåverken.

50 Wern, L., Fredriksson, U., Ring, S. (1986)
Spridningsberäkningar för lösningsmedel i Tidaholm.

51 Wern, L. (1986)
Spridningsberäkningar för Volvo BM ABs anläggning i Braås.

52 Ericson, K. (1986)
Meteorological measurements performed May 15, 1984, to June, 1984, by the SMHI.

53 Wern, L., Fredriksson, U. (1986)
Spridningsberäkning för Kockums Plåtteknik, Ronneby.

54 Eriksson, B. (1986)
Frekvensanalys av timvisa temperaturobservationer.

55 Wern, L., Kindell, S. (1986)
Luktberäkningar för AB ELMO i Flen.

56 Robertson, L. (1986)
Spridningsberäkningar rörande utsläpp av NO_x inom Fagersta kommun.

57 Kindell, S. (1987)
Luften i Nässjö.

58 Persson, Ch., Robertson, L. (1987)
Spridningsberäkningar rörande gasutsläpp vid ScanDust i Landskrona - bestämning av cyanväte.

59 Bringfelt, B. (1987)
Receptorbaserad partikelmodell för gatumiljömodell för en gata i Nyköping.

60 Robertson, L. (1987)
Spridningsberäkningar för Varbergs kommun. Bestämning av halter av SO_2, CO, NO_x samt några kolväten.

61 Vedin, H., Andersson, C. (1987)
E 66 - Linderödsåsen - klimatförhållanden.

62 Wern, L., Fredriksson, U. (1987)
Spridningsberäkningar för Kockums Plåtteknik, Ronneby. 2.

63 Taesler, R., Andersson, C., Wallentin, C., Krieg, R. (1987)
Klimatkorrigering för energiförbrukningen i ett eluppvärmt villaområde.

64 Fredriksson, U. (1987)
Spridningsberäkningar för AB Åetå-Trycks planerade anläggning vid Kungens Kurva.

65 Melgarejo, J. (1987)
Mesoskalig modellering vid SMHI.

66 Häggkvist, K. (1987)
Vindlaster på kordahus vid Alviks Strand - numeriska beräkningar.

67 Persson, Ch. (1987)
Beräkning av lukt och föroreningshalter i luft runt Neste Polyester i Nol.

68 Fredriksson, U., Krieg, R. (1987)
En överskalig klimatstudie för Tornby, Linköping.

69 Häggkvist, K. (1987)
En numerisk modell för beräkning av vertikal momentumtransport i områden med stora råhetselement. Tillämpning på ett energiskogsområde.

70 Lindström, Kjell (1987)
Weather and flying briefing aspects.

71 Häggkvist, K. (1987)
En numerisk modell för beräkning av vertikal momentumtransport i områden med stora råhetselement. En koefficientbestämning.

72 Liljas, E. (1988)
Förbättrad väderinformation i jordbruket - behov och möjligheter (PROFARM).

73 Andersson, Tage (1988)
Isbildning på flygplan.

74 Andersson, Tage (1988)
Aeronautic wind shear and turbulence.
A review for forecasts.

75 Källberg, P. (1988)
Parameterisering av diabatiska processer i numeriska prognosmodeller.

76 Vedin, H., Eriksson, B. (1988)
Extrem arealnederbörd i Sverige 1881 - 1988.

77 Eriksson, B., Carlsson, B., Dahlström, B. (1989)
Preliminär handledning för korrektion av nederbördsmängder.

78 Liljas, E. (1989)
Torv-väder. Behovsanalys med avseende på väderprognoser och produktion av bränsletorv.

79 Hagmarker, A. (1991)
Satellitmeteorologi.

80 Lövblad, G., Persson, Ch. (1991)
Background report on air pollution situation in the Baltic states - a prefeasibility study.
IVL Publikation B 1038.

81 Alexandersson, H., Karlström, C., Larsson-McCann, S. (1991)
Temperaturen och nederbörden i Sverige 1961-90. Referensnormaler.

82 Vedin, H., Alexandersson, H., Persson, M. (1991)
Utnyttjande av persistens i temperatur och nederbörd för vårflödesprognoser.

83 Moberg, A. (1992)
Lufttemperaturen i Stockholm 1756 - 1990. Historik, inhomogeniteter och urbaniseringseffekt.
Naturgeografiska Institutionen, Stockholms Universitet.

84 Josefsson, W. (1993)
Normalvärden för perioden 1961-90 av globalstrålning och solskenstid i Sverige.

85 Laurin, S., Alexandersson, H. (1994)
Några huvuddrag i det svenska temperatur-klimatet 1961 - 1990.

86 Fredriksson, U. och Ståhl, S. (1994)
En jämförelse mellan automatiska och manuella fältmätningar av temperatur och nederbörd.

87 Alexandersson, H., Eggertsson Karlström, C. och Laurin S. (1997).
Några huvuddrag i det svenska nederbördsklimatet 1961-1990.

88 Mattsson, J., Rummukainen, M. (1998)
Växthuseffekten och klimatet i Norden - en översikt.

89 Kindbom, K., Sjöberg, K., Munthe, J., Peterson, K. (IVL)
Persson, C. Roos, E., Bergström, R. (SMHI). (1998)
Nationell miljöövervakning av luft- och nederbördskemi 1996.

90 Foltescu, V.L., Häggmark, L (1998)
Jämförelse mellan observationer och fält med griddad klimatologisk information.

91 Hultgren, P., Dybbroe, A., Karlsson, K.-G. (1999)
SCANDIA – its accuracy in classifying LOW CLOUDS

92 Hyvarinen, O., Karlsson, K.-G., Dybbroe, A. (1999)
Investigations of NOAA AVHRR/3 1.6 μm imagery for snow, cloud and sunglint discrimination
(Nowcasting SAF)

93 Bennartz, R., Thoss, A., Dybbroe, A. and Michelson, D. B. (1999)
Precipitation Analysis from AMSU
(Nowcasting SAF)

94 Appelqvist, Peter och Anders Karlsson (1999)
Nationell emissionsdatabas för utsläpp till luft - Förstudie.

95 Persson, Ch., Robertson L. (SMHI)
Thaning, L (LFOA). (2000)
Model for Simulation of Air and Ground Contamination Associated with Nuclear Weapons. An Emergency Preparedness Model.

96 Kindbom K., Svensson A., Sjöberg K., (IVL) Persson C., (SMHI) (2001)
Nationell miljöövervakning av luft- och nederbördskemi 1997, 1998 och 1999.

97 Diamandi, A., Dybbroe, A. (2001)
Nowcasting SAF
Validation of AVHRR cloud products.

98 Foltescu V. L., Persson Ch. (2001)
Beräkningar av moln- och dimdeposition i Sverigemodellen - Resultat för 1997 och 1998.

99 Alexandersson, H. och Eggertsson Karlström, C (2001)
Temperaturen och nederbörden i Sverige 1961-1990. Referensnormaler - utgåva 2.

100 Korpela, A., Dybbroe, A., Thoss, A. (2001)
Nowcasting SAF - Retrieving Cloud Top Temperature and Height in Semi-transparent and Fractional Cloudiness using AVHRR.

101 Josefsson, W. (1989)
Computed global radiation using interpolated, gridded cloudiness from the MESA-BETA analysis compared to measured global radiation.

102 Foltescu, V., Gidhagen, L., Omstedt, G. (2001)
Nomogram för uppskattning av halter av PM_{10} och NO_2

103 Omstedt, G., Gidhagen, L., Langner, J. (2002)
Spridning av förbränningsemissioner från småskalig biobränsleeldning
– analys av PM2.5 data från Lycksele med hjälp av två Gaussiska spridningsmodeller.

104 Alexandersson, H. (2002)
Temperatur och nederbörd i Sverige 1860 - 2001

105 Persson, Ch. (2002)
Kvaliteten hos nederbördskemiska mätdata som utnyttjas för dataassimilation i MATCH-Sverige modellen".

106 Mattsson, J., Karlsson, K-G. (2002)
CM-SAF cloud products feasibility study in the inner Arctic region
Part I: Cloud mask studies during the 2001 Oden Arctic expedition

107 Kärner, O., Karlsson, K-G. (2003)
Climate Monitoring SAF - Cloud products feasibility study in the inner Arctic region.
Part II: Evaluation of the variability in radiation and cloud data

108 Persson, Ch., Magnusson, M. (2003)
Kvaliteten i uppmätta nederbördsmängder inom svenska nederbörskemiska stationsnät

109 Omstedt, G., Persson Ch., Skagerström, M (2003)
Vedeldning i småhusområden

110 Alexandersson, H., Vedin, H. (2003)
Dimensionerande regn för mycket små avrinningsområden

111 Alexandersson, H. (2003)
Korrektion av nederbörd enligt enkel klimatologisk metodik

112 Joro, S., Dybbroe, A.(2004)
Nowcasting SAF – IOP
Validating the AVHRR Cloud Top Temperature and Height product using weather radar data
Visiting Scientist report

113 Persson, Ch., Ressner, E., Klein, T. (2004)
Nationell miljöövervakning – MATCH-Sverige modellen
Metod- och resultatsammanställning för åren 1999-2002 samt diskussion av osäkerheter, trender och miljömål

114 Josefsson, W. (2004)
UV-radiation measured in Norrköping 1983-2003.

115 Martin, Judit, (2004)
Var tredje timme – Livet som väderobservatör

116 Gidhagen, L., Johansson, C., Törnquist, L. (2004)
NORDIC – A database for evaluation of dispersion models on the local, urban and regional scale

117 Langner, J., Bergström, R., Klein, T., Skagerström, M. (2004)
Nuläge och scenarier för inverkan på marknära ozon av emissioner från Västra Götalands län – Beräkningar för 1999

118 Trolez, M., Tetzlaff, A., Karlsson, K-G. (2005)
CM-SAF Validating the Cloud Top Height product using LIDAR data

119 Rummukainen, M. (2005)
Växthuseffekten

120 Omstedt, G. (2006)
Utvärdering av PM_{10} - mätningar i några olika nordiska trafikmiljöer

121 Alexandersson, H. (2006)
Vindstatistik för Sverige 1961-2004

122 Samuelsson, P., Gollvik, S., Ullerstig, A., (2006)
The land-surface scheme of the Rossby Centre regional atmospheric climate model (RCA3)

123 Omstedt, G. (2007)
VEDAIR – ett internetverktyg för beräkning av luftkvalitet vid småskalig biobränsleeldning
Modellbeskrivning och slutrapport mars 2007

124 Persson, G., Strandberg, G., Bärring, L., Kjellström, E. (2007)
Beräknade temperaturförhållanden för tre platser i Sverige – perioderna 1961-1990 och 2011-2040

125 Engart, M., Foltescu, V. (2007)
Luftföroreningar i Europa under framtida klimat

Sveriges meteorologiska och hydrologiska institut
601 76 Norrköping · Tel 011-495 8000 · Fax 011-495 8001
www.smhi.se

ISSN 0283-7730